INFORMATION TO USERS

The most advanced technology has been used to photograph and reproduce this manuscript from the microfilm master. UMI films the text directly from the original or copy submitted. Thus, some thesis and dissertation copies are in typewriter face, while others may be from any type of computer printer.

The quality of this reproduction is dependent upon the quality of the copy submitted. Broken or indistinct print, colored or poor quality illustrations and photographs, print bleedthrough, substandard margins, and improper alignment can adversely affect reproduction.

In the unlikely event that the author did not send UMI a complete manuscript and there are missing pages, these will be noted. Also, if unauthorized copyright material had to be removed, a note will indicate the deletion.

Oversize materials (e.g., maps, drawings, charts) are reproduced by sectioning the original, beginning at the upper left-hand corner and continuing from left to right in equal sections with small overlaps. Each original is also photographed in one exposure and is included in reduced form at the back of the book.

Photographs included in the original manuscript have been reproduced xerographically in this copy. Higher quality 6" x 9" black and white photographic prints are available for any photographs or illustrations appearing in this copy for an additional charge. Contact UMI directly to order.

U·M·I

University Microfilms International
A Bell & Howell Information Company
300 North Zeeb Road, Ann Arbor, MI 48106-1346 USA
313/761-4700 800/521-0600

Order Number 9020822

Time-resolved studies of light scattering in random media

Yoo, Kwong Mow, Ph.D.

City University of New York, 1990

U·M·I
300 N. Zeeb Rd.
Ann Arbor, MI 48106

A

Time resolved studies of light scattering in random media

by

K. M. Yoo

A dissertation submitted to the Graduate Faculty in Physics in partial fulfillment of the requirements for the degree of Doctor of Philosophy, The City University of New York.

1990

This manuscript has been read and accepted for the Graduate Faculty in Physics in satisfaction of the dissertation requirement for the degree of Doctor of Philosophy.

2/8/90
Date

Chairman of Examining Committee

2/6/90
Date

Executive Officer

Supervisory Committee

The City University of New York

Abstract

Time resolved studies of light scattering in random media

by

K. M. Yoo

Advisor: R. R. Alfano

The goal of this thesis is to study photon migration and light scattering in random media. The backscattering and transmission of an ultrafast laser pulse in random media were measured by a time and angle resolved technique using ultrafast laser and streak camera technology.

The angular and temporal information of the light backscattered from random media was measured simultaneously. Weak photon localization which is due to coherent interference of the multiply scattered light and its time reverse counterpart was observed in the scattered femtosecond laser pulse. The angular width of the coherent peak was shown to become narrower as the light undergoes a longer scattering path in the random medium. The intensity of the backscattered pulse in the exact backward direction is higher than those scattered in other directions. The temporal profile of the backscattered pulse can be characterized by the transport mean free path and the absorption length. The temporal and angular profiles of the backscattered

light can be used to determine the optical properties of biological and medical tissues. This backscattering technique is a potentially noninvasive medical diagnostic tool. The dynamics of depolarization of light scattering in random media were measured and can be important for determining the size of the particle in the random media.

In the experiment on ultrafast laser propagation through a slab of random media, the coherent and incoherent components of forward light scattering were time resolved. The pulse width and the direction of the coherent component remain unchanged. The incoherent component has a wide angular and temporal spread. The diffusion approximation fails to describe the temporal spread of the incoherent component when the thickness of the random medium is less than ten transport mean free paths.

Acknowledgement

The patient guidance of Professor R. R. Alfano and help from members of IUSL and PAL during the course of this research are gratefully acknowledged.

This research was made possible from financial and educational support provided in part by Hamamatsu Photonics K.K., HYPRES Inc. and MediScience Technnology Corporation.

Table of Contents

Abstract iii

Acknowledgement v

List of figures ix

I Weak photon localization 1

1.1 Introduction 1

1.2 Theory 3

1.3 Experimental method 8

1.4 Results and discussion 10

1.4.2 Time and angle resolved studies of the coherent peak 11

1.5 Conclusion 13

II Temporal profile of the backscattered pulse 14

2.1 Introduction 14

2.2 Theory 14

2.3 Experimental method 16

2.4 Results and discussion 16

2.5 Conclusion 19

III Time resolved depolarization of multiple backscattered light from random media 20

3.1 Introduction 20

3.2 Theory 21

3.3 Experimental method 23

3.4 Results and discussion 23

3.5 Conclusion 27

IV Characterization of the biological tissue from the backscattered light 28

4.1 Introduction 28

4.2 Resolution and limitation of methods 30

4.3 Results and discussion 31

4.3.a Heart 32

4.3.b Tooth 32

4.3.c Cataract eye 33

4.3.d Breast and lung tissues 34

4.3.e Leaf 35

4.4 Conclusion 36

V Time resolved coherent and incoherent component of forward light scattering in random media 37

5.1 Introduction 37

5.2 Experimental method 38

5.3 Results and discussion 38

5.4 Conclusion 43

VI When does the diffusion approximation fail to describe photon transport in random media? 45

6.1 Introduction 45

6.2 Theory 46

6.3 Experimental method 47

6.4 Results and discussion 47

6.5 Conclusion 50

VII Summary and Future directions 51

7.1 Summary 51

7.2 Future directions 52

7.2a Photon localization 52

7.2b Pulse propagation 53

7.2c Microscopic medium characterization 54

Appendices 55

Figures 74

References 106

List of Figures

1.1 Light scattering in random medium 74

1.2 Experimental setup 75

1.3 Coherent backscattering of 80 fs laser pulse 76

1.4 Coherent backscattered pulses of 80 fs laser pulse 77

1.5 Angular and temporal profile of the backscattered pulse 78

2.1 Temporal profiles of the backscattered pulses for various l_i 79

2.2 Temporal profiles of the backscattered pulses for various l_a 80

2.3 Backscattered pulses for different amount of dye 81

2.4 Backscattered pulses for different amount of beads 82

2.5 Backscattered pulses from 1% of latex beads 83

3.1 FWHM of polarized backscattered pulses 84

3.2 Polarized backscattered pulses: Experiment 85

3.3 Polarized backscattered pulses: Theory 86

4.1 Backscattered pulses from a heart 87

4.2 Backscattered pulses from a tooth 88

4.3 Coherent backscattering from a tooth 89

4.4 Backscattered pulses from an cataract eye 90

4.5 Theoretical fit to the backscattered pulse from an eye 91

4.6 Coherent backscattering from a breast tissue 92

4.7 Coherent backscattering from a lung tissue 93

4.8 Coherent backscattering from a lung tissue at different times 94

4.9 Backscattered pulses from a lung tissue at two angles. 95

4.10 Backscattered pulses from a breast tissue at two angles. 96

4.11 Coherent backscattering from a leaf 97

5.1 Angle and time information of transmitted pulses 98

5.2 Angle and time information of transmitted pulses 99

5.3 Plot of I_c / I_t versus z / l_s 100

5.4 Transmitted pulses: theory and experiment 101

6.1 Experimental setup 102

6.2 Transmitted pulse profiles: experimental results and diffusion theory (d = 0.296 μm) 103

6.3 Transmitted pulse profiles: experimental results and diffusion theory (d = 3.136 μm) 104

6.4 Average time of arrival $\bar{t}$ versus z / l_t 105

Chapter I

Weak photon localization

1.1 Introduction

When a photon, i.e. light, encounters a varying dielectric constant medium, its direction of propagation changes. The degree of scattering of light by a particle depends on: the size of the particle with respect to the wavelength, the refractive index of the particle with respect to the background, and the shape of the particle. A quantitative measurement of the degree of scattering is the scattering cross section σ_s which is given by

$$\sigma_s = \int f(\theta) d\Omega , \tag{1.1}$$

where $f(\theta)$ is the scattering amplitude of the light as a function of angle θ, and $d\Omega$ is the integration over all angle. A particle much smaller than the wavelength of the light scatters the light in all direction, and the scattering cross section can be approximated by the Rayleigh equation. The scattering cross section of a particle on the order of a wavelength is computed by Mie theory. For a large particle the light is scattered mostly in the forward direction (anisotropic scattering) within an angle of $1.2\lambda / d$, where d is the diameter of the particle, and the scattering cross section is approximately equal to the geometric cross section ($\pi(d/2)^2$)of the particle. The amplitude of the scattered light depends on the angle. The momentum transfer scattering cross section σ_m is a quantitative measurement of the light scattering away from the forward direction. The light scattered at a bigger angle is counted more than those scattered at a smaller angle by multiplying the scattering amplitude $f(\theta)$ by a scaling factor $(1-\cos(\theta))$. That is,

$$\sigma_m = \int f\ (\theta)(1-\cos(\theta))d\ \Omega \tag{1.2}$$

This angular scaling reduces the value of σ_m with respect to σ_s if the light is scattered in the forward direction.

When light enters a many particle system of particle concentration n, the transport of light in this medium depends on the following parameters: (1) the transport mean free path l_t, $l_t = 1/(n\ \sigma_m)$, the distance between scattering events (bigger angle); (2) the scattering mean free path l_s, $l_s = 1/(n\ \sigma_s)$, the distance between scattering; and (3) the absorption length l_a, the mean distance the light propagates before it is being absorbed.

When light enters a disordered medium, it is inevitably scattered randomly. Until recently, an important property of light transport has not been seriously taken into consideration; that is, the path of light propagation in a random medium possesses the property of time reversal symmetry. This symmetry gives rise to the phenomenon of weak localization[1-4] of light scattering in random media.

Weak localization arises from the coherent interference between the scattered light and its time-reversed counterpart. This interference enhances the intensity of the scattered light within a small angular cone in the backward direction. The angular profile of the intensity enhancement around the backward direction is often referred to as the coherent peak. The angular lineshape of the coherent peak is almost triangular in shape, with the peak occurring in the exact backward direction. The intensity of the peak is nearly twice the intensity of the constant background scattering. The width of the coherent peak[5] (measured from the peak to the bottom of the coherent peak) is approximately equal to $\frac{\lambda}{2\pi l_t}$, where λ is the wavelength of the scat-

tered light. The constant background intensity arises from the diffuse light scattering.

In this chapter the phenomenon of weak localization was studied using an ultrafast laser for which the angular and temporal profile of the backscattered pulse from random media were obtained simultaneously. The angular profile of the coherent peak is found to become narrower as the light is scattered through a longer path length in the random medium. The intensity of the scattered pulse in the exact backward direction was found to be enhanced due to coherent interference. The temporal profile of the backscattered pulse can be characterized in terms of the transport mean free path and absorption length.

1.2 Theory

The intensity of light scattered from a random medium is obtained by the solution to the wave equation and has been worked out by a number of people[4-12]. To calculate the scattered intensity, let us consider a ray with wavevector $\vec{k}_i$ incident on the medium which is being scattered first at position $\vec{x}_i$. This ray then undergoes a series of scatterings before it is finally scattered out of the medium at $\vec{x}_f$ with wavevector $\vec{k}_f$. Let this scattered field be given by $\vec{E}(\vec{x}_i, \vec{k}_i; \vec{x}_f, \vec{k}_f)$. Similarly, another ray of wavevector $\vec{k}_i$ is first scattered at position $\vec{x}_l$, and then undergoes a series of scatterings before it is finally scattered out at $\vec{x}_m$ with wavevector $\vec{k}_f$. The intensity of light scattered at an angle θ (angle between $-\vec{k}_i$ and $\vec{k}_f$) is given by summing the square of all the scattered fields which can be written as

$$I(\theta) = \sum_{i,f,l,m} \vec{E}(\vec{x}_i, \vec{k}_i; \vec{x}_f, \vec{k}_f)\, \vec{E}^*(\vec{x}_l, \vec{k}_i; \vec{x}_m, \vec{k}_f)$$

$$e^{i(\vec{k}_i \cdot \vec{x}_i - \vec{k}_f \cdot \vec{x}_f) - i(\vec{k}_i \cdot \vec{x}_n - \vec{k}_f \cdot \vec{x}_m)} \tag{1.3}$$

This summation can be split into the following three terms:

$$I(\theta) = \sum_{x_i, x_f} \vec{E}(\vec{x}_i, \vec{k}_i; \vec{x}_f, \vec{k}_f)\, \vec{E}^*(\vec{x}_i, \vec{k}_i; \vec{x}_f, \vec{k}_f) \tag{1.3a}$$

$$+ \sum_{x_i, x_f} \vec{E}(\vec{x}_i, \vec{k}_i; \vec{x}_f, \vec{k}_f)\, \vec{E}^*(\vec{x}_i, \vec{k}_i; \vec{x}_f, \vec{k}_f)\, e^{i(\vec{k}_i + \vec{k}_f)\cdot(\vec{x}_i - \vec{x}_f)} \tag{1.3b}$$

$$+ \sum_{i \neq f \neq l \neq m} \vec{E}(\vec{x}_i, \vec{k}_i; \vec{x}_f, \vec{k}_f)\, \vec{E}^*(\vec{x}_l, \vec{k}_l; \vec{x}_m, \vec{k}_f)$$

$$e^{i(\vec{k}_i \cdot \vec{x}_i - \vec{k}_f \cdot \vec{x}_f) - i(\vec{k}_l \cdot \vec{x}_n - \vec{k}_f \cdot \vec{x}_m)} \tag{1.3c}$$

These three terms represent the scattering in Figs. 1.1 (a), (b), and (c) respectively. The first term is a purely diffuse scattering and the scattered intensity has no angular dependence. The second term has taken the time reversal symmetry into account where $\vec{E}^*(\vec{x}_f, \vec{k}_i; \vec{x}_i, \vec{k}_f) = \vec{E}^*(\vec{x}_i, \vec{k}_i; \vec{x}_f, \vec{k}_f)$. This assumption holds as long as the time reversal symmetry is not destroyed along the scattering trajectories, which is true in most media except in the presence of a magnetic field, where the time reversal symmetry is destroyed and produces Faraday rotation. This term contributes to the coherent interference in the backward direction (weak localization) and the scattered intensity is determined by the phase shift $(k_i + k_f)\cdot(x_i - x_f)$. This coherent interference is the only important interference that exists for light scattering from dense random media.

The last term [eq. (1.3c)] describes completely random interference. This gives rise to a large intensity fluctuation and is normally observed in laser scattering from solid random media.[13,14] By rotating or shaking the solid medium, the large fluctuation of scattered intensity disappears, and a smooth coherent peak and constant background appear. This is due to the fact that

the rotation gives an ensemble average over a large number of different configurations, where the fluctuations of the scattered light represented by equation 1.1(c) cancel one another. In the case of particles dispersed in liquid, the random Brownian motion of the suspended particles acts as a natural dynamics for many different configurations of particle distribution. For micro size latex beads suspended in water, the time taken for rearrangement is in the order of milliseconds. Thus, the angular intensity profile obtained in a few second is rather smooth because of ensemble averaging.

The angular width of the coherent peak is $\theta \approx \frac{\lambda}{2\pi l_t}$. Consequently, the medium with larger transport mean free path would have a narrower coherent peak. In the case of latex beads suspended in water, the transport mean free path at 10% volume concentration of $0.33\mu m$ latex beads suspended in water is about $20\mu m$.[15] The angular width of the coherent peak is about $5mrad$. In some stronger scattering media such as titania and silica particles, a transport mean free path as short as $0.35\mu m$ has been observed.[16]

It has been realized that the coherent peak is due to the sum of contributions from scattered light traveling through different path lengths. The coherent width is broadest for a light beam which undergoes just two scatterings, and the width becomes narrower as the light beam travel through longer scattering paths. This phenomenon can be understood as follows:[5,8,11,17] the phase shift between the two counter-propagating waves is given by $(\vec{k}_i + \vec{k}_f)\cdot(\vec{x}_i - \vec{x}_f)$. The condition for constructive interference can be approximated by

$$\theta k \mid \vec{x}_i - \vec{x}_f \mid < 1 \qquad (1.4)$$

where θ is the angle between $-\vec{k}_i$ and $\vec{k}_f$, and k is equal to $\mid k_i \mid$. In the

diffusion approximation the distance $|\vec{x}_i - \vec{x}_f|$ is determined by the total distance the light travels in the medium L and the transport mean free path l_t, and is given by

$$|\vec{x}_i - \vec{x}_f| = \sqrt{l_t L / 3} \tag{1.5}$$

A derivation of eq. (1.5) is located in appendices A1. Thus, for light scattered through a distance L in the medium, constructive interference for light scattering occurs within a cone having an angle of inclination of

$$\theta < \frac{1}{k\sqrt{l_t L / 3}}. \tag{1.6}$$

The angular width of the cone would decrease for light undergoing longer scattering paths. Using the time-resolved method,[19] one can resolve the contribution to the coherent peak from one particular pathlength. This type of work will be described in detail later.

Using a cw laser, the cumulative contributions of light scattered through different pathlengths have been studied by other groups[15,17] who used thin slabs of various thicknesses w. In these experiments the distance L the light travels is given by

$$L < \sqrt{3w / l_t} \tag{1.7}$$

would contribute to the line shape of the backscattered light; that is, it integrates over all the pathlengths which are less than L. Taking the difference between two slabs yields the contribution to the line shape for pathlengths between L_1 and L_2.

Another recent experiment used dyes in the scattering medium[17-18] to study localization. In this case, the light which travels through long scattering paths has a higher probability of being cut off by absorption. As the

concentration of the dye increases, the coherent peak becomes rounder because the long scattering paths which contribute to the narrow peak are being cut off by the absorbing dye.

The coherent interference also exists for light scattered with polarization perpendicular to the incident laser (cross polarization).[8,15,20-22] The lineshape and the enhancement of the coherent peak for cross-polarization are different from the case of parallel polarization and depends on the size of the scatterers. The enhancement is generally smaller and the lineshape is broader in the case of cross-polarization.

The line shape of the coherent peak can be quantitatively described by[5,10]

$$\alpha(\theta) = \frac{3}{16\pi}[1+2\frac{z_0}{l_t} + \frac{1}{(1+ql_t)^2}(1+\frac{1-e^{-2qz_0}}{ql_t})], \tag{1.8}$$

where θ is the angle of the scattered light measured from the exact backward direction, $q = 2\pi\theta / \lambda$, and z_0 is determined by the boundary condition, in a plane interface $z_0 \approx 0.7 l_t$.

To calculate the temporal profile of the scattered light, the intensity of the scattered light in the direction $\hat{s}$ is

$$I(\hat{s}, t) = \int dt' \; R(\hat{s}, t') \, I_0(t - t') \tag{1.9}$$

where $I_0(t - t')$ is the incident pulse, and $R(\hat{s}, t')$ is the response function of the random medium. In the diffusion approximation one can write[7,8]

$$R(\hat{s}, t') = \alpha \frac{1}{\sqrt{2\pi}} e^{D_0 t' / 2 l_t^2} D_{-3}(\sqrt{2 D_0 t' / l_t^2}) \tag{1.10}$$

where α is a proportional constant, l_t is the transport mean free path, $D_{-3}(x) = u(\frac{5}{2}, x)$ is the parabolic cylinder (Weber) function,[23] $D_0 = cl_t / 3$ is the diffusion constant, and c is the effective speed of the wave in the medium. Equation (1.10) corresponds to diffuse scattering and is independent of the scattering angle. Theoretically, it corresponds to the sum of ladder diagrams in the calculation of the 2-photon Greens function. To include coherent interference due to time reversal symmetry in the scattering process, one should take the maximal crossed-diagrams into account.[4,5,7] The sum of the maximal crossed-diagrams will result in a factor of $e^{-D_0 q^2 t'}$ in equation (1.10), where $q = \frac{2\pi}{\lambda} \sin\theta$, and θ is the angle $\hat{s}$ makes with the backward direction of the incident light. This term accounts for the coherent interference between scattered waves propagating in the time reversed path in the random medium, and exhibits the following important characteristics. The intensity at $\theta = 0$ is highest and is a factor of two greater than the diffusive intensity ($\theta = 0$ corresponds to the exact backward direction). The final expression for the intensity of the scattered pulse is

$$I(\hat{s}, t) = \alpha \frac{1}{\sqrt{2\pi}} \int dt' \; R(\hat{s}, t') \left(1 + e^{-D_0 q^2 t'}\right) I(t - t') \qquad (1.11)$$

If the random medium is absorbing with an absorption length l_a, then an absorption factor of e^{-vt / l_a} should be included in the integrand of eq. (1.11).

1.3 Experimental Method

A schematic of the experimental set up is shown in Fig. 1.2. A $80 fs$ laser pulse at a repetition rate of 82 Mhz was generated from an argon laser pumped, colliding pulse mode-locked dye laser with four prisms for chirp

compensation. The laser wavelength is 620 nm and the bandwidth is 12 nm. The beam of 3 mm diameter was collimated through a distance of 20 m. The laser was incident on the random medium after reflection from a beam splitter.

The random media studied were polystyrene spheres of various diameters suspended in water at various concentrations. The suspended latex beads were contained in a glass cell of dimension 10 *mm* ×10 *mm* ×30 *mm* which could be considered as semi-infinite media. The normal of the front surface of the glass cell was placed at a small angle with the incident laser such that the direct reflected light was rejected from the detector. The scattered light from the media was collected by a lens with a 800 mm focal length. The detecting slit of the Hamamatsu 3-dimensional synchroscan streak camera (8 ps resolution) video system was placed at the focal plane of the collecting lens. Thus, each position on the slit corresponds to a given scattering angle. The synchroscan streak camera was set in the operating mode and was triggered externally by a photodiode activated by the laser. Both the angular distribution as well as the temporal information on the intensity of the scattered light were obtained simultaneously. The data was acquired by accumulating a total of 1.2×10^8 laser shots in 15 seconds which was stored and analyzed by a computer. The angular resolution was 0.3 *mrad* which is due to limitations imposed by the finite beam size (diffraction), laser divergence, and alignment.

1.4 Results and discussion

1.4.1 Weak localization in the femtosecond time domain

The experimental results for the backscattered lineshape using 80 femtosecond pulses are shown in Fig. 1.3. The two curves shown correspond to volume concentrations of 10% and 1% of diameter 0.33 μm latex beads suspended in water. The sample preparation is described in Appendix A2. Both the incident laser and the detector polarizer were polarized in the horizontal direction. These lineshapes were similar to the result from a similar cw laser experiment, using a cw He-Ne laser. For detection with the polarizer placed in the vertical direction, there was a small enhancement. These observation are in agreement with theory and cw experiments.

In these experiments, the 10% concentration sample has a transport mean free path of about 20 μm which corresponds to a time between each scattering event of about 90 fs. In the case of the 1% concentration, the transport mean free path is about 140 μm which corresponds to a time scale of 620 fs. Considering a particular scattering trajectory where the light undergoes 10 scattering events, the total time taken is about 6.2 ps. The two counter-propagating rays overlap at the middle of the trajectory, and the duration of time in which they overlap and interfere is equal to the pulse width, which is 80 fs, or on the order of 9 μm in space. At other times, the two rays propagate independently. These two counter-propagating light waves overlap and interfere again at the detector where they are collected by the converging lens at the focal plane. This overlapping time (80fs) is small compared with the total time (6.2 ps) the photons spend inside the medium. Thus, the interference between the two counter-propagating waves inside the medium

is negligible and can be excluded. In fact, in the time-resolved method using a streak camera, the coherent interference up to 45 ps was observed. In a steady state experiment where the counter-propagating waves are always continuous along a given scattering trajectory, one cannot eliminate the interference between waves inside the medium which may affect our observation. Consequently, the observed coherent peak in the weak localization regime is due to coherent interference outside the medium at the point of observation.

In the above discussion, we have assumed that when a laser pulse is spread into a bundle of microrays inside the scattering medium, the pulse width of each of these microrays remains the same as the original laser pulse. The laser pulse can become broader because of group velocity dispersion which can be a serious problem for the waves scattered through a long distance. Nevertheless, for those ray propagating in time less than 100 ps the pulse broadening does not pose a serious problem.

Using a femtosecond pulse experiment, we conclude that the phenomenon of weak localization is indeed due to the interference outside the medium at the point of observation between the scattered light and its time-reversed counterpart. The interference among the counter-propagating rays inside the medium has a negligible effect on scattered light in the regime of weak localization.

1.4.2 Time- and angle-resolved studies of the coherent peak

Figure 1.4 shows the intensity of a backscattered laser pulse as a function of time at two different angles. The scattered intensity was obtained from a 1% volume concentration of polystyrene spheres of diameter 0.33 μm

suspended in water. The time axis is taken with reference to the peak of the incident pulse at the boundary which is at 0 ps. The peak of the scattered pulse was displaced by about 4 ps after the incident pulse. Curve (a) is the backscattered laser pulse at 0 mrad, and curve (b) is at 5 mrad. The coherent interference between the scattered light and its time-reversed counterpart, causes the enhancement in intensity at 0 mrad, and can be easily observed up to 45 ps which corresponds to a pathlength of 10 mm, above which the two curves merge. In this case, the angular width of the coherent peak is estimated to be 0.3 mrad. This value is calculated from eq. (6) using $l_t = 140\ \mu m$, $L = 10\ mm$, $\lambda = 620\ nm$. Above 45 ps the angular width of the coherent peak become smaller than 0.3 mrad. The detecting system of the streak camera sees the light intensity smeared out over an angular width of 0.3 mrad. It is this fact that causes the two curve to merge.

Figure 1.5 shows the lineshapes of the backscattered light detected at various times after the incident pulse enters the random medium. The curves in this figure show that the width of the coherent peak is larger at shorter times. The width at 0 ps is twice that of 4 ps. The width becomes narrower as the light undergoing longer scattering pathlength. The curves also show the relative intensity contributing to the coherent peak from the various scattering pathlengths.

Using time-resolved techniques, we have observed directly the contribution from different scattering pathlengths to the coherent peak of backscattered light from a random medium.

1.5 Conclusion

The phenomenon of weak photon localization was observed with ultrafast laser pulse as short as 80 fs. The coherent peak is due to interference between the counterpropagating light pulses at the point of observation. The simultaneous measurement of angular and temporal information of the backscattered pulse directly shows that the angular width of the coherent peak becomes narrower as the light undergoes longer scattering paths in the random media. The intensity of the backscattered pulse is enhanced around the exact backward direction because of coherent interference.

Chapter II

Temporal profile of the backscattered pulse

2.1 Introduction

The optical characteristics of random media can be quantitatively described in terms of three parameters: the scattering mean free path, the transport mean free path, and the absorption length of the light traveling in the media. In this chapter we show that these parameters can be obtained directly from a temporal profile of the backscattered pulse. [19,26-29]

2.2 Theory

In a weakly scattering medium, the intensity of the backscattered pulse decays exponentially in time: this will be described later.[29] This exponential decay indicates that the backscattered pulse may be described by a single exponential function. The beam intensity at position x inside the medium is

$$I(x,t) = I_0 \, e^{-x(1/l_s + 1/l_a)} \delta(x - vt), \tag{2.1}$$

where I_0 is the incident intensity and l_s and l_a are the attenuation lengths due to scattering and absorption, respectively. The backscattered intensity at position x is proportional to $I(x,t)$ and is further reduced by a factor of $e^{-x(1/l_s + 1/l_a)}$ when the light propagates out of the medium. The backscattered intensity from the position x is

$$I_b(x,t) = \alpha I_0 e^{-2x(1/l_t + 1/l_a)} \delta(2x - vt), \tag{2.2}$$

where α is related to the backscattering cross section and the concentration of the beads. Thus, the intensity of backscattered light at time t measured by the streak camera is given by

$$I_b(t) = \alpha I_0 e^{-vt(1/l_t + 1/l_a)}. \tag{2.3}$$

Equation (2.3) holds if most of the detected light undergoes single scattering.

In a strongly scattering medium, the multiple scattering of light may be approximated by diffusion theory. The temporal profile of the backscattered pulse has been derived previously and is given by equation (1.11). The temporal profile of the backscattered pulse is determined by the transport mean free path l_t and the absorption length l_a. For large l_t, the time interval between scattering is also large, resulting a broader temporal profile of the backscattered pulse. As an illustration, the temporal profiles of the backscattered pulses are computed from equation (1.11) and plotted in Fig. (2.1) for l_t = 50, 500, 5000, and 50000 μm, and $l_a = \infty$ which is the case of non-absorbing medium. The temporal profile has been convoluted with the impulse response of the detecting system. The impulse response is taken as Gaussian profile with 8ps FWHM which is the typical impulse response function of the present synchroscan streak camera.

In an absorbing medium, light that undergoes long scattering path lengths or coming back at later time have a higher probability of being cut off. The reduction in intensity at later time increases as the absorption length decreases. Figure (2.2) illustrates the temporal profiles with different absorption lengths l_a of 500, 2000, 5000, and 50000 μm, for $l_t = 200 \mu m$.

2.3 Experimental method

Ultrafast laser pulses of $80\,fs$ (repetition rate $82\,MHz$, $\lambda = 620\,nm$, beam diameter $3\,mm$) were generated from a colliding pulse mode-locked dye laser system. The laser was incident upon the random medium after reflection from a beam splitter. The other portion of the beam was used as a reference pulse to monitor the arrival time of the scattered pulse. The back-scattered pulse from the random medium, after passing through two apertures of $4\,mm$ diameter $1\,m$ apart, was collected into the streak camera. The distance between the random medium and the streak camera detection was approximately 1.7 m which is significantly larger than the thickness (0.026 m) of the random medium. In this experimental geometry the backscattered light within $4\,mrad$ is detected, and the solid angle of detection of the light scattered from the front and the back portion of the random medium is the same.

The random medium consists of latex beads suspended in water in a rectangular glass cell (2 cm by 3.5 cm by 2.6 cm). The latex beads have negligible absorption. The normal to the front surface of the cell was tilted at an angle of 3^{o} with respect to the laser beam, so that the direct reflected beams at the interfaces were excluded from the detector. The temporal profiles of the backscattered pulse were studied for various bead diameters and concentrations and different absorbing dye (Malachite green) concentrations.

2.4 Results and discussion

The intensities of the backscattered pulse versus time on linear and semi-log plots are shown in Fig. 2.3 for latex beads of 0.091 μm diameter in the weakly scattering regime. The zero time is taken at the arrival of the direct

reflected pulse at the random medium and glass interface. The peak at 232 ps is the small angle scattering in the medium of the direct reflected pulse at the back interface of the cell. As the absorbing dye was added into the sample, the scattered pulse decayed faster, as illustrated in Fig. 2.3(a). The semilog plots of the curves in Fig. 2.3(a) are shown in Fig. 2.3(b). $-(1/\ l_s + 1/\ l_a)\log_{10} e$ is the gradient of the slope on the semilog plots of Fig. 2.3(b). Since $v\ /\ l_a$ is proportional to dye concentration, a plot of $v\,(1/\ l_s + 1/\ l_a)$ versus the dye concentration should yield a linear curve. This linear dependence is verified in the inset in Fig. 2.3(a) where a plot of $v\,(1/\ l_s + 1/\ l_a)$ versus dye concentrations is presented. However, the points in the Inset of Fig. 2.3(b) at higher dye concentrations deviate from the linear lines.

When no dye was added to the media, the attenuation lengths from the temporal profile were calculated to be 18 and 12 mm for media with a 0.106% concentration of 0.091 μm diameter latex beads and a 0.076% concentration of 11.9 μm diameter latex beads, respectively. These lengths are equal to l_s because l_a is much longer. The scattering mean free path $l_s{}^m$ can be theoretically computed from Mie theory by $l_s{}^m = 1/\ (n\ \sigma_s)$, where n is the number density and σ_s is the scattering cross section. In the case of a 0.106 $\pm$ 0.003 % concentration of 0.091 μm diameter latex beads, $l_s{}^m = 1/\ (n\ \sigma_s)$ is calculated to be 10.7mm, with the use of the number density of $n = 2.7 \times 10^{18} m^{-3}$ and the scattering cross section $\sigma_s = 3.48 \times 10^{-17} m^2$ computed from Mie theory. Similarly, $l_s{}^m = 4.7mm$ for the case of a medium with a 0.076% concentration 11.9 μm diameter latex beads. The scattering lengths obtained from the experiment (18 and 12 mm) are larger than but of the same order of magnitude as their respective values computed from Mie theory

(10.7 and 4.7 mm) for the cases of media with small ($0.091\mu m$) and large ($11.9\mu m$) beads, respectively. This disagreement indicates that the scattering mean free path computed from Mie theory $l_s{}^m$ is a crude approximation for the scattering attenuation constant l_s obtained from the temporal profile of the backscattered pulse. The attenuation constant l_s is a measure on the intensity reduction because of light scatters away from the forward direction.

In the medium where 0.15 ml of absorbing dye solution was added to 14.15 ml of a 0.106% concentration of $0.091\mu m$ diameter beads, the absorption length l_a is calculated to be 18 mm from the temporal profile. In the other medium where $0.15ml$ of Malachite green solution was added to 14.11 ml of medium with a 0.076% concentration of $11.9\mu m$ diameter latex bead suspension, the absorption length calculated from the temporal profile is 19 mm. The absorption length at 620 nm for the same concentration of the dye solution without the beads was independently measured from the transmission geometry with a spectrometer and was found to be 29 mm. This value is of the same order as the absorption length obtained from the temporal profile of the backscattered pulse. The above analysis is valid for weakly scattering media where the detected scattered light is dominated by single backscattering events.

Figure 2.4(a) illustrates the change of temporal profiles for increasing concentrations of latex bead of $0.091\mu m$ diameter. The semilog plots in Fig. 2.4(b) show that the decaying portion of the scattered intensity deviated from a linear line at higher concentrations because of multiple light scattering in the random medium. Equation (2.3) no longer describes the backscattered pulse profile. The backscattered pulse is described by eq. (1.11).

The transport mean free path (the scattering length) and the absorption length can be separated and obtained from the backscattered pulse profile in the strongly scattering regime. To illustrate this, the backscattered pulse from a 0.91% volume fraction of a 0.46 μm diameter bead medium is presented in Fig. 2.5(a). The curve with a faster decay time has some absorbing dye added, and the other curve has no dye added. Using eq. (4) to fit the experimental data in Fig. 2.5(a), we found that l_t is 260μm and that the l_a for the media without and with the dye solution added is 80×10^3 and 20×10^3 μm, respectively. From Mie theory, $l_t = 1/(n\,\sigma_m)$, where σ_m is the momentum exchange scattering cross section. Given that $n = 1.78\times10^{17} m^{-3}$ and $\sigma_m = 2.17\times10^{-14} m^2$, $l_t = 260\mu m$, which is in agreement with the fitted values obtained above. Theoretical curves for stronger absorbing media are shown in Fig. 2.5(b) with $l_a = 5\times10^3$ and 0.5×10^3 μm.

2.5 Conclusion

We showed that the scattering and absorption lengths can be separately obtained from the temporal profile of the backscattered pulse. Thus, the optical properties of a random medium can be determined from the temporal profile of the backscattered pulse.

Chapter III

Time resolved depolarization of multiple backscattered light from random media

3.1 Introduction

The dynamical polarization nature of light has not been carefully studied, partly because of the experimental and mathematical complexity in dealing with the Stokes parameters[32] for polarization of the multiple scattered light from random media. Nevertheless, polarization is an important property that could be utilized to investigate the phenomena of light scattering and to yield the characteristics of random media. The depolarization of the light scattering in random media depends on the size of the scatterers, the angle of scattering and the number of scattering events. These dependences produce significant differences between the temporal intensity distributions for parallel and perpendicular polarization components of light backscattered from random media with different particle sizes. Understandably, a number of phenomena of multiple light scattering in random media, such as weak photon localization[1-4,8,20,34-36], temporal[37,38] and spatial[39,40] intensity-intensity correlation depends on the polarization. The polarization dependence arises primarily because these phenomena depend on the intensity distribution of the scattered light propagating through different pathlengths[10,15,17,41] or

on the number of scattering events in the random media. This chapter introduces time resolved femtosecond technology to study the dynamics of depolarization of light backscattered from random media with different particle sizes and concentrations.

3.2 Theory

Quantitatively, the backscattered pulse from a random medium is given by [26]

$$I(t) = \int dt' R(t') I_0(t - t') \tag{3.1}$$

where $I_0(t - t')$ is the incident pulse and $R(t')$ is the impulse response function of the random medium. In the diffusion approximation [26]

$$R(t) \quad \alpha \quad e^{D_0 t / 2 l_t^2} D_{-3}(\sqrt{2 D_0 t / l_t^2}) e^{-vt / l_a} \tag{3.2}$$

where l_t is the transport mean free path, $D_{-3}(x) = u(5/2, x)$ is the parabolic cylinder (Weber) function, $D_0 = c l_t / 3$ is the diffusion constant, c is the light velocity in the random medium, and l_a is the absorption length of the light in the media. The coherent interference due to weak photon localization is neglected because we are measuring at an angle of 6^0 where coherent interference is negligible.

To take the polarization into account, the backscattered pulse intensity at time t can be split into two components defined by parallel and perpendicular polarization coefficients: $C^{//}(t)$ and $C^{+}(t)$. The parallel and perpendicular polarization of backscattered pulses are written as [31]

$$I^{//}(t) = C^{//}(t) I(t) \tag{3.3a}$$

and

$$I^{+}(t) = C^{+}(t)\, I(t). \tag{3.3b}$$

Assuming Rayleigh scattering, the strengths of parallel and perpendicular polarization after n scattering events are approximated by [8,10,35]

$$p^{//}(n) = \frac{1 + 2\,(0.7)^{n-1}}{2 + (0.7)^{n-1}} \tag{3.4a}$$

and

$$p^{+}(n) = \frac{1 - (0.7)^{n-1}}{2 + (0.7)^{n-1}}. \tag{3.4b}$$

These equations show that the light depolarizes completely after n=20 scattering. The number of scattering the photon experiences after time t can be described by a parameter vt / l_s : the distance the photon travel (vt) divided by the scattering mean free path (l_s). In random media, the number (n) of scattering events the photon encounters after a time t is most likely to follow the Poisson distribution. The probability that the photon experiences n scattering events after time t is given by

$$P_n(t) = \frac{(vt / l_s)^n}{n!} \frac{1}{e^{(vt / l_s)} - 1} \tag{3.5}$$

where integer $n \geqslant 1$. Thus, the polarization coefficients at time t are

$$C^{//}(t) = \sum_{n=1}^{\infty} p^{//}(n)\, P_n(t) \tag{3.6a}$$

and

$$C^{+}(t) = \sum_{n=1}^{\infty} p^{+}(n)\, P_n(t). \tag{3.6b}$$

All of these equations plus a convolution for the 8ps temporal resolution of the streak camera are used to compute the temporal profiles of the backscattered pulses. The transport and scattering mean free path used are computed

by Mie theory from the given particle diameters and concentrations.

3.3 Experimental method

Laser pulses of 80 fs at a repetition rate of 82 MHz were generated from a colliding pulse mode-locked dye laser. These laser pulses were collimated to a beam diameter of 5 mm and were polarized in the horizontal direction. A prepulse was used as a reference pulse to mark the zero time of the backscattered pulse and to monitor the intensity of the incident pulse. The laser pulse backscattered at a small angle of 6 ± 1^0 with specular direction was collected into a Hamamatsu synchroscan streak camera after passing through two collimating pinholes of 2mm in diameter. An analyzer was placed in front the streak camera to select the horizontal (parallel) or vertical (perpendicular) polarization component of the backscattered pulse. The random medium consisted of latex beads suspended in water. The depolarization of the backscattered pulse were studies with various beads of diameters smaller, almost equal, and larger than the wavelength of the incident light which is $0.620\mu m$ in air or $0.465\mu m$ in water. The volume concentration of the latex beads started with 10% and then diluted by a factor of 10.0 ± 0.3, 100 ± 6, ...

3.4 Results and discussion

The intensity distribution of backscattered light can be characterized by the fullwidth at half maxima (FWHM) of the backscattered pulse. Fig. 3.1 plots the FWHM of the backscattered pulse versus the particle concentrations for three different media consisting scatterers with diameters of: 0.460 ± 0.005, 0.091 ± 0.006, and 3.134 ± 0.004 μm. These diameters are approximately equal to, smaller than, and larger than the wavelength of the light,

respectively. Significant differences in the FWHM are observed between the parallel and the perpendicular polarization components of the backscattered pulse from these three media. When the diameter comparable to the laser wavelength, the temporal profile for both parallel and perpendicular polarization components of the backscattered pulse are similar at all concentrations as shown in Fig. 3.1(a). In the case where the scatterer size is much smaller than the laser wavelength, the temporal profile for the perpendicular polarized pulse is significantly broader than the parallel polarized pulse at all concentrations. In the other limiting case where the scatterers are much larger than the wavelength of the laser, the perpendicular polarized pulse is broader than the parallel polarized pulse at low particle concentrations but their scattering pulse profiles becomes similar at higher particle concentration. This interesting observation that the dependence on the scatterer sizes and concentrations on the FWHM of parallel and perpendicular components of the backscattered pulse points out the importance of time-resolved ultrafast laser technology to characterize the optical properties of random media. This time resolved depolarization technique could also added to our understanding of light propagation and scattering in medical and biological media.

Figs. 3.2 (a), (b), (c), and (d), show the experimental results of backscattered pulse intensity in time from different random media. The salient feature of the temporal profiles for parallel (solid curves) and perpendicular (dotted curves) polarized pulses from four different random media consisting latex beads of 0.091 ± 0.006, 0.296 ± 0.010, 3.134 ± 0.004, and 11.9 ± 1.9 μm diameters, respectively. A substantial amount of polarization is preserved at early times and eventually completely depolarized at later time where the parallel and perpendicular intensity merge. The polarization during earlier

times comes from low order scattering where most of the polarization is preserved. At later time the light has undergone many scattering events and becomes depolarized. In the case of a medium with small particles, one can show from Rayleigh scattering[35] that the light become completely depolarized after as many as 20 scattering events. As shown from the measurements, the ratio of the intensity of perpendicular to parallel polarization component of the backscattered pulse are: smallest for media with particle size much smaller than the laser wavelength, highest for particle size on the order of the wavelength, and become smaller for particle much bigger than the wavelength. This different amount of polarization preservation can partly be accounted for by the dependence of the angular distribution of the scattered light on the size of the scatterers. A bead of diameter d scatters the light mainly in the forward direction within an angle of $1.2\lambda / d$: The angle of scattering decreases as the size of the bead increases. In a random medium with larger beads, more number of scattering events are required to turn the light around in the backward direction. The large number of scattering events depolarizes the light. To illustrate that the rate of depolarization increases with the size of the particle, let us look at the backscattered pulse profiles presented in 10% of Fig. 3.3(a), 1% of Fig. 3.3(b), and 10% of Fig. 3.3(c). These have about the same transport mean free paths which are 120, 230, and 330 μm , respectively. These curves show that the intensity of the depolarized (perpendicular polarization) pulse is becoming equal to the intensity of the polarized (parallel polarized) pulse as the size of the bead increases. However, when the bead is very large, there is a substantial amount of backscattering in addition to the forward scattering. A significant amount of polarization is preserved because of a large number of single backscattering event.

The above formulation should hold for particle of size much smaller than the wavelength of the light in which eq. (3.4) is valid. Indeed, the theoretical plots for the case of 0.091 μm diameter beads presented in Fig. 3.3(a) closely resemble the experimental results shown in Fig. 3.2(a). It is not certain that the formulation above can be applied to larger diameter scatterers because the Rayleigh scattering does not apply. Nevertheless, the backscattered pulse profile were computed for parallel and perpendicular polarization components. Comparing the experimental results in Fig. 3.2 and the corresponding theoretical plots in Fig. 3.3, the above theory and experiment are in qualitative agreement and are especially good for higher concentration media. A better theory is needed for larger particle.

There are some deviations between the prediction of the above theory and the experimental results. The intensity of the perpendicular polarization components are slightly bigger in the experimental results compare to that of theory for the case of latex beads of 0.296 μm diameter. A primary factor could be the scattered light depolarized faster for particles of size close the wavelength of the light than that expected from the Rayleigh scattering represented by equation (3.4). A significant amount of polarization is preserved in later times in the experiment than the theory predicts, which is particularly obvious in the case of media at lower concentrations and larger particles. This unexpected amount of polarization may be accounted by single backscattering signal from deep inside the media where the parallel polarization is maintained. This single backscattering is not accounted by the diffusion approximation but is an important source of backscattering signal for big particle. Comparing the backscattered pulses plotted in fig. 3.2(d) and 3.3(d), as the concentration of the particle decreases from 10% to 1% and then

to 0.1%, the temporal profiles from the experiment do not broaden as much as predicted by the theory. This shows that the parameters $l = 1/ n \sigma_m$ is not good for the case of large particle, where σ_m is the momentum exchange scattering cross section. This failure of description is caused by a substantial amount of single backscattering from large particle.

3.5 Conclusion

We have shown that the temporal profile of parallel and perpendicular polarized backscattered pulse from small particle media can be described by the Rayleigh formulation. The intensity of the perpendicular polarized pulse is becoming equal to the intensity of the parallel polarized pulse as the size of the bead increases, given that their transport mean free path is the same. When the bead is very large, there is a substantial amount of backscattering in addition to the forward scattering. Thus a significant amount of polarization is preserved because of a large number of single backscattering events.

Chapter IV

Characterization of the biological tissues from the backscattered light

4.1 Introduction

This chapter explores some novel applications of an ultrafast laser and detection technology or/and weak photon localization in life science, such as to characterized and diagnose biological materials.

The optical properties of biological and medical materials can be quantitatively measured in terms of two scattering parameters: the transport mean free path l_t, and the absorption length l_a of the light traveling in the media. These scattering parameters determine the degree of photon migration in tissues. The phenomenon of weak photon localization is observed in biological tissues and could be used to determined the scattering characteristics of the tissues. The backscattered light can be used as a technique to differentiate various tissue, such as to diagnose cancer from the state of normal and benign tissues.

The scattering and absorption parameters can be directly used to determine the state of the biological material. The absorption length l_a is the distance the light propagates in the medium before it is absorbed. It depends on the wavelength of the light. It also depends on the chemical composition of

the medium: the absorption cross section and the concentration of the absorbing chemical present in the medium. Thus, a change in absorption length indicates a change in chemical composition in the biological material. The transport mean free path l_t is the mean distance the light travel between scattering. In a random medium, l_t is simply related by $1/\ n\ \sigma_m$, where n is the number density and σ_m is the momentum exchange scattering cross section of the particle or cell. The σ_m depends on the size of the particle relative to the light wavelength and the refractive index of the particle. If the arrangement of the particles in the medium is correlated, the light may not be scattered as much as it would be in a complete random medium. This reduction in scattering is due to the correlation of the phase of the scattered light which reduces the amount of scattering. The light will have a longer transport mean free path in a medium where the particles are correlated. A change in the state of the material, such as dehydration, would result a change in number density, particle size, particle-particle correlation, and aggregation of particles. These changes would result in different l_t.

In the past, the parameters l_t and l_a were obtained from continuous wave[25] or ultrafast pulse transmission experiments[24]. The main disadvantages of the transmission technique are: (1) it requires a measurement of the thickness of the samples, (2) it may not be feasible for bulk sample because the transmitted energy can become too weak to be detected, and (3) it measures the average properties of the slab through which the light propagate rather than the optical properties over a thin penetration epth. These disadvantages do not exist when using the backscattering technique. Furthermore, the backscattering technique is a non-invasive technique using a fiber array..

4.2 Resolution and Limitation of methods

The experimental technique for measuring the angular and temporal profile of the light backscatters from biological tissues is similar to that described in the earlier chapters and is shown schematically in Fig. 1.2. These methods are limited to range of length that can be measured accurately.

The temporal profile of a backscattered pulse from a perfect measuring system is given by eq. (1.11). The finite time response of the streak camera in measuring the temporal profile of the backscattered pulse limit our capability of determine optical properties of random medium with short transport mean free path. The full width at 1/e maxima of the pulse (eq. (1.11)) backscattered from medium with transport mean free path 300 μm is 1 ps. This full width at 1/e maxima (FW1/eM) decreases as the transport mean free path decreases. The time response of the present synchroscan streak camera is about 8 ps, which could be difficult to determine the pulse width of less than 1 ps. However, the presence of a long tail in the temporal profile of the backscattered pulse (Fig. 2.1) can held us to differentiate the backscattered pulse smaller than 1 ps FW1/eM. Thus, a 8 ps time response synchroscan streak camera cannot be used to determine the optical properties of a random medium with transport mean free path of less than 100 μm,. Determination of shorter transport mean free path require a better time resolution. Better time resolution can be achieved by using a single short streak camera which has a time response of 0.5ps. Better time resolution can also be achieved by a cross-correlation technique such as Kerr gate, second harmonic generation and two photon generation, where their time response is determined by the pulse width of the laser.

The angular width of the coherent peak of the backscattered light decrease as the transport mean free path increases. The angular width is about 0.3 mrad when the transport mean free path is 500 μm, computed from eq. (1.8). The diffraction of light because of finite beam size is $1.2\lambda/d$, where d is the diameter of the beam. The usual beam size of the laser is $d = 4\ mm$, and the wavelength of the laser is $\lambda = 620\ nm$. The diffraction of the light is 0.2 *mrad* full width at half maxima (FWHM) which limits our capability to measure an angular profile of the less than 0.3*mrad* FWHM.

The limitations in measuring l_t due to finite time response and angle response of the instrument are complementary. The 8ps time response limits our capability to determine l_t for values smaller than 100 μm from fitting the temporal profile. While with an angle response of 0.3 mrad one can easily determine l_t equal or smaller than 100 μm from fitting the angular profile of the backscattered light. However, with 0.3 mrad angle response one cannot determine l_t with value greater than 500μm from the angular profile. But this large l_t value can be determined from the temporal profile of the scattered pulse.

4.3 Results and discussion

The following section illustrates the the versatility of the techniques to various medical and biological applications using temporal and angular profiles of ultrafast laser pulses backscattering for several biological or medical media.

4.3.a Heart

Fig. 4.1 illustrates the backscattered pulse from two different tissues in the heart: the fat tissue deposited on the heart and the heart tissue itself. Their temporal profiles are different and one can easily distinguish between them. The temporal profile of the fat is shorter but with a longer tail, indicating shorter l_t and longer l_a. These is reasonable because the fatty portions are white and absorb light less strongly compared to heart tissue which contains absorbing hemoglobin. From a fit of the curves using theory of equation (1) to (3), l_t and l_a are found to equal $600\mu m$ and $30000\ \mu m$ for fat tissue, and $800\ \mu m$ and $15000\ \mu m$ for heart tissue at $620nm$, respectively.

4.3.b Tooth

Fig. 4.2 plots a series of backscattered pulses from different portions of a human tooth. The scattered pulse from the top portion of the tooth is plotted in Fig. 4.2(a). From fitting of the temporal profile to the theory, we obtain $l_t = 3.2 \pm 2mm$ and $l_a = 85 \pm 5mm$. The temporal profiles from the root of the tooth show a double peak and a much shorter tail. The short tail indicates that the scattered light in being cut off at some later time because of the finite thickness of the tooth. The light scattered out from the other side will be lost. Because of refractive index mismatch at the second tooth-air interface. Light is scattered back and detected by the streak camera as a second peak. The temporal distance between the two peaks can be used to estimate the optical thickness or the refractive index of the medium. The angular profile of the backscattered light from the tooth are presented in Fig. 4.3. This example shows that the tooth or bone has a rather long l_t of 3.2 mm which allows possible application of laser to see through bone instead of X-

ray.

4.3.c Cataract eye

The backscattered intensity of a laser pulse as a function of time, for a clear, partially cataracted, and severely cataracted eye are shown in Figs. 4(a), (b), and (c), respectively. The cataracts are artificially induced on the bovine eye lens by submerging the eye in saline solution containing hydrogen peroxide. The two peaks shown in Figs. 4(a) and (b) arise from scattering off the front and the back interfaces between the eye lens and the saline solution. The temporal separation δt between these two peaks is approximately 40ps. The thickness of the lens d can be computed from this time separation $d = c\,\delta t\,/\,2n_g$, where c is the speed of light and n_g is the refractive index of the lens. The thickness of the lens is computed to be about $4mm$, which is in fair agreement with the actual lens thickness.

In a clear eye, there is very little scattering in the lens. Only scattering at the interfaces is observed, as shown by the two clear peaks in Fig. 4.4(a). As the eye develops a cataract, some of the light is scattered inside the eye lens. This scattering reduces the ratio of the intensity of the back to the front peak as illustrated in Fig. 4.4b. This decrease in ratio is a measure of the extent of scattering in the lens and hence increasing opacity due to formation of cataracts. For a severely cataract eye, the light undergoes multiple scattering and the diffusion approximation for light scattering holds. The experimental data in Fig. 4.4(c) can be fit to the theory. The best fit between the experiment and theory is plotted in Fig. 4.5 The transport mean free path and absorption length are found to be $200 \pm 50\mu m$ and $30 \pm 5mm$, respectively. The absorption length is 150 times longer than the transport mean free path.

This measurement shows that the attenuation due to absorption is significantly smaller than that due to scattering at λ=620nm .

4.3.d Breast and lung tissues

Fig. 4.6 shows the angular distribution of the scattered laser intensity from a human breast tissue. The coherent peak is clearly seen. A similar effect but with a wider coherent peak was observed in human benign lung tissue which is shown in Fig. 4.7. The transport mean free path l_t , and the absorption length l_a can be obtained by fitting the experimental data with equations (4) to (7) convoluted with the angular resolution of detection. For the breast tissue, the best fit to the experimental data of the coherent peak occurs when $l_t = 250 \pm 30\mu m$ and $l_a = 4000 \pm 1000\mu m$. In the case of lung tissue, $l_t = 80 \pm 20\mu m$ and $l_a = 3000 \pm 1000\mu m$ for the best fit. The theoretical fits are traced by smooth solid lines in the figures. The coherent peak for lung tissue is broader than that of breast tissue, which shows that the lung tissue is a stronger light scattering medium than that of breast tissue. Quantitatively, the light has a shorter l_t in lung tissue $l_t = 80\mu m$ than in the breast tissue $l_t = 250\mu m$.

It has been shown that the coherent peak become narrower as the light scatters through a longer distance in the random medium.[17,15,28] This is also observed in biological tissue which is shown by an example for light scattering in cancerous lung tissue. The intensity and the line shape of the coherent peak of the scattered light at various times after the incident pulse is plotted in Fig. 4.8. The intensity of the peak compared with the constant background is less than a factor of two. One of the primary reasons is due to finite angular resolution of the detecting system. Note that in Fig. 4.8 the coherent peak

disappears at times greater than 22ps. At time greater than 22 ps, the angular width of the coherent peak is estimated to be less than 0.4 mrad. This angular width is comparable to the angular resolution of our detecting system and thus the coherent peak is not observed.

The temporal profiles of the scattered pulse at two angular regions, coherent (at 0mrad) and diffuse (at 3mrad) regions, for normal breast and lung tissues are shown in Figs. 4.9 and 4.10, respectively. The intensity of the scattered light in the coherent region is greater than that in the diffuse region in the early times. The profiles merge at later times. The scattered pulse from the breast cancer tissue (Fig. 4.10) is broader than that from the lung cancer tissue (Fig. 4.9). This indicates the transport mean free path of the light is longer in the breast tissue, which is in qualitative agreement with the results obtained from the line shape of the coherent peak.

The best fit to the experiment data for breast tissue shown in Fig. 4.10 is when $l_t = 1.6 \pm 0.3mm$ and $l_a = 20 \pm 4\ mm$. The best fit for lung tissue is shown in Fig. 4.9, $l_t = 350 \pm 50\ \mu m$ and $l_a = 16 \pm 4\ mm$. These lengths are very similar to the values obtained in the transmission geometry by Navarro and Profio[25]. However, these lengths are significantly longer than those obtained from the angular line shape, which needs to be further addressed and studied.

4.3.e Leaf

Finally, we illustrate an example in photosynthesis using the angular profile of the coherent peak to probe the absorption property of a leaf at 620nm [see Fig. 4.11]. There is no coherent peak for light backscattered from the green leaf. A clear coherent peak is observed when chlorophyll of the

leaf is then extracted by submerging the leaf in methanol for a day. These results are presented in Fig. 4.11. By fitting this coherent peak, l_t and l_a are found to be equal to $70 \pm 15\mu m$ and $1800 \pm 400\mu m$, respectively. The absence of coherent peak for a green leaf show that the chlorophyll absorbs light at 620nm very efficiently. The l_a is about $150 \pm 50\mu m$. This approach can be used to measure the absorption spectrum at low levels in highly scattering media.

5.4 Conclusion

Weak photon localization has been observed in biological tissues. The transport mean free path and the absorption length of the light in tissues can be determined either from the line shape of the coherent peak $I(\theta)$ or the temporal profile $I(t)$ of the backscattered pulse. The absorption length can be obtained from the slope of $\log I(t)$ versus t at later time. The transport mean free path can be obtained by fitting $\log I(t)$ versus t curve from which l_t longer than $100\ \mu m$ can be determined using $8ps$ impulse response synchroscan streak camera. The time-resolved backscattering technique using streak camera and ultrafast laser will be versatile probe on biological materials since most material have l_t longer than $100\mu m$. The coherent peak can be used to determined l_t when it is shorter than $500\ \mu m$. The temporal profile of the backscattered pulse has a potential to monitor the extent of cataract development in the eye, and to differentiate different states of biological tissues.

Our findings show that time and angle resolved backscattering of light may find important application in medical diagnosis and investigation of various biological system.

Chapter V

Time Resolved Coherent and Incoherent Components of Forward Light Scattering in Random Media

5.1 Introduction

The propagation and scattering of light waves in random media have interested physicists for over a century because of their practical importance in medicine, communication, imaging, remote sensing, and spectroscopy. An analytical solution to the wave equation for pulse propagation and distortion in a random medium in the intermediate scattering regime remains one of the most challenging problems in modern physics. A laser pulse enters a random medium will undergoes multiple scattering. The coherent interference among the multiple scattered light in the forward direction forms the coherent component. And those scattered randomly in all direction forms the incoherent component. This chapter presents first experimental results to our knowledge on the pulse distortion in the intermediate regime, where the coherent (ballistic) pulse coexists with the incoherent (diffusive) pulse in the forward direction. The temporal profile of the scattered pulse was found to be described by the diffusion theory[24,42] when the thickness of the medium is greater than ten transport mean free paths. The approximate solutions obtained by Ishimaru nd Hong[43,44] are in qualitative but not quantitative agreement with

the experimental results.

5.2 Experimental method

A colliding pulse mode-locked dye laser system generated 80 fs pulses (λ 620 nm, repetition rate 82 MHz, laser power 5 mW). The laser beam is expanded to 30mm in diameter and is allowed to propagate through a slab of random medium consisting of latex beads suspended in water in a glass cell 40mm in diameter. A black pinhole 2.5mm in diameter was placed on the opposite side of the glass cell along the laser path. This experimental setting may be approximated as a plane wave propagating through a slab of random medium. Temporal and angular information of the light scattered out from the pinhole was measured simultaneously using streak camera. The experimental angular and temporal resolutions are 1$mrad$ and 8ps, respectively. A reference pulse was set to monitor the arrival time.

5.3 Results and discussion

Figures 5.1 and 5.2 show the salient temporal and angular information of the scattered light pulse after it passed through a 10 mm slab of random media. The first white spot in Figs. 5.1 and 5.2 denotes the reference pulse. Only a coherent pulse (the second spot) is observed at low particle concentrations, where $n\ \sigma_s\ z \leqslant 15$, with n the number density, σ_s the scattering cross section computed from the Mie theory, and z the thickness of the slab. The pulse width of the coherent pulse measured by the streak camera remains the same within the resolution of 8 ps (Figs. 5.1 and 5.2). An additional component distinct from the coherent component begins to appear [Fig. 5.1(b)] when the particle concentrations were increased above $n\ \sigma_s\ z \geqslant 16$. The large

temporal and angular spreads of the second component clearly indicate that this component arises from the light being multiply scattered in the random media.

The range of the number density of the latex beads for a given diameter at which the two components coexist was narrow and within an order of magnitude. For example, the ranges were $1 - 6 \times 10^{12}\ m^{-3}$, and $6 - 10 \times 10^{16}\ m^{-3}$, for latex bead diameters d of 15.8 and 0.33 μm, respectively. The particle number density in this intermediate regime differs widely with different particle diameters; by 4 orders of magnitude between $d = 15.8\mu m$ and $d = 0.33\ \mu m$. However, the parameter $n\ \sigma_s$ can be used as a good scaling parameter, based on the experimental results for latex beads of diameters $d = 0.33, 0.46, 3.134$, and $15.8\ \mu m$. The plots of the ratio of the coherent to the total scattered intensity I_c / I_t versus $n\ \sigma_s\ z$ in Fig. 5.3 clearly show that the coherent intensity drops rapidly, within an order of magnitude, where $15 \leqslant n\ \sigma_s\ z \leqslant 25$, independent of the size of the scatterers. The onset of the rapid drop of I_c / I_t depends on the solid angle of collection f. By diffusion approximation one can obtain

$$\frac{I_c}{I_t} = \frac{1}{1 + f\ (e^{n\ \sigma_s\ z} - 1) / (1 + n\ \sigma_m\ w)} \tag{5.1}$$

where σ_m is the momentum transfer scattering cross section computed by Mie theory.

The temporal displacement between the coherent and incoherent peaks decreases as the size of the scatterers increases and the thickness of the random medium decreases. This displacement is as large as 20 ps for latex beads of small diameter ($d = 0.33\mu m$) and decreases rapidly to 2 and 0 ps ($1ps$ resolution) for beads diameters of $3.134\mu m$ and $15.8\mu m$, respectively. These

features are presented in Figs. 5.1(d) and 5.2. It is also shown that the temporal spread of arrival times for the incoherent component is narrower for a larger bead medium (Fig. 5.2) and broader for a smaller bead medium [Fig. 5.1(d)]. This is expected because the larger bead scatters the light mainly in the forward direction, whereas the smaller bead scatters the light in all directions.

The transition from coherent to incoherent scattering is presented in Fig. 5.1 for a slab $10mm$ thick and a bead diameter of 0.33 μm. At a low concentration of scatterers, up to $n = 7.0\times10^{16} m^{-3}$ ($n\ \sigma_s\ z = 17.9$), only the coherent component is visible [Fig. 1(a)]. The incoherent component becomes visible at a slightly higher concentration [Fig. 1(b)] where $n = 8.0\times10^{16}\ m^{-3}$ ($n\ \sigma_s\ z = 20.4$). The incoherent component rapidly gains in intensity relative to the coherent counterpart as the concentration increases [Figs. 5.1(c) - (e)]. The corresponding bead concentrations are $n = 8.9$, 9.5, and $10.4\times10^{16}\ m^{-3}$ where $n\ \sigma_s\ z = 22.8$, 24.3, and 26.8, respectively. When $n\ \sigma_s\ z$ is above 26, only the incoherent component is visible. Fig. 5.1(f) shows a typical diffusive scattering characteristic for a particle concentration of $17.3\times10^{16} m^{-3}$ with $n\ \sigma_s\ z = 44.6$.

The temporal intensity distribution of the incoherent component of our experimental geometry predicted by the diffusion theory[42] is given by

$$I_z(t) = \frac{D}{\pi w^2} \sum_{m=1}^{\infty} m\,(\pi w / d)^2 \sin(m\,\pi w / d) \exp(-Dt\,(m\,\pi / d)^2) \quad (5.2)$$

where $w = 10mm$ is the thickness of the slab, $D = v l_t / 3$ is the diffusion coefficient, $d = w + 2z_0$, $z_0 = 0.71\ l_t$, and l_t is the transport mean free path. The diffusion approximation is valid when w / l_t is much greater than 1 and is expected to break down as w / l_t becomes smaller. The following

procedure is used to check where the modified diffusion equation fails to describe the experimental data. The transport mean free path l'_t for a high-particle-concentration n' medium is obtained by fitting the diffusion equation to the experimental data. Then, the transport mean free path l_t for a lower particle concentration n medium is obtained from

$$l_t = l'_t \, n' \, / \, n \tag{5.3}$$

if the diffusion approximation is still valid. The pulse profile is computed from the diffusion equation [eq.(5.2)] using this l_t and is then compared to the experimental data. For the case [d=3.134 μm] presented in Fig. 5.4(a), $n = 3.17 \times 10^{14} m^{-3}$ and $l_t = 1.52 mm$, which is computed from eq. (5.3) using $n' = 6.03 \times 10^{14} m^{-3}$, $l'_t = 0.8 mm$. The predicted pulse profile from the diffusion theory is plotted by the solid curve in Fig. 5.4(a). Similarly, the data of the smaller diameter [0.296 μm] case are presented in Fig. 5.4(b) for $n = 2.18 \times 10^{17} m^{-3}$ and $l_t = 1.1 mm$, which are computed from eq. (5.3) using $n' = 9.75 \times 10^{17} m^{-3}$, $l'_t = 0.24 mm$. These experimental data show an earlier photon arrival than that predicted by diffusion theory. The deviation of the computed diffusion curve from the experimental data increases as l_t increases. These results show that the diffusion approximation is not valid in this regime. One of the factors for the earlier photon arrival is the anisotropic scattering. The particle of diameter d scattered the light mainly in the forward direction within an angle of λ / d, which effectively reduces the time for the photon to propagate through the slab of random media.

Approximate analytical solutions obtained by Ishimaru and Hong[43] take the anisotropic scattering into account. With a two-frequency mutual coherence function Γ and the Rytov approximation, where $\Gamma_1 = \exp(\psi)$, the output pulse is given by

$$I(t) = T\frac{\omega_r}{\sqrt{2\pi}}\int_0^\infty \exp(-(Tw_r x)^2/8)\, A(x)\cos(\phi(x) - w_r x\, t)\, dx \quad (5.4)$$

$$A(x) = \exp[-n\,\sigma_t\, z\,(1-(W_0/x)\tan^{-1}x)] \quad (5.5)$$

$$\phi(x) = (n\,\sigma_t\, z/2)[(W_0/x)\ln(1+x^2)] \quad (5.7)$$

$$x = \omega_d/\omega_r\ , \quad \omega_r = 2\alpha v/z\ , \quad W_0 = \sigma_s/\sigma_t$$

where T is the FWHM of the incident pulse, t is the time where the zero is set at the arrival of the laser pulse through the medium without scatterers, and σ_t is the total scattering cross section and is equal to σ_s for a nonabsorbing particle. The value $\alpha = 2.5(d/\lambda)^2$ is related to the scattering amplitude; v is the phase velocity in the medium, and x and w_d are integration variables. $A(x)$ decays to a constant value, $e^{-n\,\sigma_t\, z}$, for large x. This constant value contributes to a coherent component of the scattered pulse.

With eq. (5.4) for the case of Fig. 5.4(a) ($d = 3.134\mu m$, $n\,\sigma_s\, z = 42.6$), the computed output pulse width and the time delay of the peak are 2.5 and $4.0ps$, respectively. The pulse profile of the computed curve is plotted by the dashed curve in Fig. 5.4(a). The computed photon curve arrives too early. The value of α may be too large. In the case of a smaller diameter ($d = 0.296\mu m$, $n\,\sigma_s\, z = 33.5$), the computed output pulse is displayed by dashed curve in Fig. 5.4(b), which also differs significantly from the experimental result (the dotted curve).

An attempt to fit the experimental curves in Figs. 5.4(a) and (b) failed for all possible values of $n\,\sigma_s\, z$, W_0, and ω_r. In particular, the theoretical results do not exhibit the long tail distribution of arrival times. This may be the result of neglecting the nonlinear term in solving the differential equation for ψ,[44] and a bad approximation for α. Nevertheless, this theory does show

some qualitative agreements. It contains the coherent component. The pulse width of the incoherent component increases with a larger $n\ \sigma_s\ z$ or smaller bead diameter (α), and the peak of the incoherent pulse is further away from zero for larger $n\ \sigma_s\ z$ or smaller bead diameters (α).

If we include the nonlinear term in the differential equation for ψ and assume that $n\ \sigma_s\ z \gg 1$, the output pulse is given by[44]

$$I(t) = \frac{\pi\omega_c}{4} \sum_{m=0}^{\infty} (2m+1)(-1)^m \exp\left[-\left((2m+1)\frac{\pi}{4}\right)^2 \omega_c\, t\right], \qquad (5.7)$$

where the coherence bandwidth $\omega_c = 8\alpha\ \nu\ /\ n\ \sigma_s\ z^2$. For $d = 3.134\ \mu m$ and $n\ \sigma_t\ z = 42.6$, the computed output pulse width and peak delay time are 3.5 and $1.4ps$, respectively. The computed pulse profile is plotted by the dashed-dotted curve in Fig. 5.4(a), which is also far from agreement with the experimental result. Again the value of α may be overestimated. In the case of a smaller diameter ($d = 0.296\ \mu m$), with $n\ \sigma_s\ z = 33.5$, the computed output pulse is displayed by the dashed-dotted curve in Fig. 5.4(b) and bears a closer resemblance to the experimental result. The failure to fit the experimental curves for extremes of particle sizes (d= 3.134 and $0.296\mu m$) and theoretical approximations ($n\ \sigma_s\ z \leqslant 1$ and $n\ \sigma_s\ z >> 1$) reveals the deficiency in the approximations obtained by Ishimaru and Hong[43,44].

5.4 Conclusion

Coherent and incoherent components of ultrafast laser pulses passing through a slab of random medium have been time resolved. The ability to time resolve the coherent from incoherent components may be important in medical imaging and diagnostics. The theory from the two frequency mutual coherence function with Rytov approximation does not give a good prediction

of the distribution of arrival times. The experimental results show that a better theoretical description of scattered pulse profile in the intermediate scattering regime is required.

Chapter VI

When does the diffusion approximation fail to describe photon transport in random media?

6.1 Introduction

Diffusion theory is widely used to describe the transport of particles and waves in random media. The analytical solutions for the diffusion equation are generally available and are found to be valid[24,42] when $z / l_t \gg 1$, where z is the thickness of the random medium, and l_t is the transport mean free path. For many physical media the particle or wave transport often occurs in the region where z / l_t is small. This is particularly true for the ultrasmall electronic devices of nanometer size, where electron traverse only a few transport mean free paths. Recently, the diffusion approximation has been extensively used in many of the pioneering light scattering studies[5,8,12,20,24,39,46] and applications of light scattering to the study of physical and biological media.[37,38,47,48] It is important to know at what value of z / l_t the diffusion approximation begins to fail. In this chapter, the transport of photons through a slab of random medium is *directly* studied using ultrafast laser pulse and time-resolved detection. Here, we provide the first direct insight on when and how the diffusion approximation deviates from the actual transport of photon through a slab of random medium. My results

resolve the current controversy[37,38,47] on whether or not photon transport is diffusive after passing through a slab of random medium of thickness only a few transport mean free paths. Weitz et al. using diffusing-wave spectroscopy[47] technique showed that photons are diffusive after propagating through a few transport mean free path thick slab. However, the results of Freund et al.[37] using a similar technique gave a contrary conclusion in which they claimed the possibility of ballistic transport. The temporal studies presented here directly show that the prediction of diffusion approximation deviates monotonically from the measured scattered pulse as the value of z / l_t decreases below 10. The scattered photons are found to arrive much earlier than predicted by the diffusion approximation. The ballistic photon transmission has been shown to exist in a small diameter random bead medium in chapter V.[48]

6.2 Theory

A direct method to probe the transport of photon in a random medium is to measure the distribution of photons in the time domain. When a plane front ultrafast pulse is incident normally onto a slab of random medium, the temporal distribution of photon arrival at a point on the opposite side of the slab is predicted by diffusion theory[42] to be

$$I_z(t) = \frac{D}{\pi z^2} \sum_{m=1}^{\infty} m (\pi z / d)^2 \sin(m \pi z / d) \exp(-Dt (m \pi / d)^2) \quad (6.1)$$

where $D = v l_t / 3$ is the diffusion coefficient, $d = z + 2z_0$, $z_0 = 0.71\, l_t$, v is the speed of photon, z and l_t have been defined earlier.

6.3 Experimental method

Our experimental arrangement is schematically shown in Fig. 6.1. closely imitates the geometry governed by eq. 1. Ultrafast laser pulses of 100 fs were generated at a repetition rate of 82 MHz from a colliding pulse mode-locked dye laser system. The laser power was 10 mW at a wavelength centered at 620 nm. The laser beam of 4 mm diameter was split into two beams: a reference beam to mark the zero time of the signal beam which was expanded to 35 mm diameter. The centered portion of the expanded laser beam was selected by a diaphragm and passed through the random medium consisting latex beads suspended in water contained in a cylindrical glass cell of 50 mm in diameter and 10 mm thick. Photons scattered out of the cell will be lost, resembling an absorbing boundary. A black pinhole of 2 mm diameter was placed at the center on the opposite side of the cell. The temporal distribution of the photon scattered out from this pin hole in the forward direction was measured by a synchroscan streak camera. The diameter of the incident beam was set to 20 mm ; any further increase in the beam diameter will not change the pulse profile of the scattered photon. The measured scattered pulse profile can be described by eq. (6.1), if the diffusion approximation is valid.

6.4 Results and discussion

Experimental studies were carried out on random media for different bead diameters, each with a series of bead concentrations. At highly concentrated random media where $z / l_t \gg 1$, the diffusion equation holds which was not surprising. In this case, the transport mean free path can be and was obtained by fitting the scattered pulse given by equation (6.1). Fig. 6.2(a)

illustrates an example where the diffusion theory fits the experimental data. The photon transport mean free path l_t was found to be 0.309 mm which is close to 0.25 mm computed from Mie theory using $l^m{}_t = 1/(n\,\sigma_m)$, where n is the number density and σ_m is the momentum transfer scattering cross section.

The following procedure is used to determine where the diffusion theory fails to describe the photon transport when z / l_t is decreased. The transport mean free path l_t for a smaller particle concentration n medium is extrapolated from a higher particle concentration n' with known transport mean free path l'_t by

$$l_t = l'_t\, n' / n \quad . \tag{6.2}$$

The scattered pulse profiles for various values of l_t is computed from the diffusion theory (eq.(6.1)). These computed pulse profiles are then compared with the experimental results of the corresponding number density.

Figs. 6.2 and 6.3 displays a series of transmitted pulse profiles for decreasing beads concentration for bead diameters of 0.296 and 3.134 μm, respectively. The curves show the diffusion theory (broken and dash-dot curves) fit the experimental data (solid curves) when z / l_t is greater than 10. Figs. 6.2(b) and 6.3(b), where $z / l_t \approx 10$, clearly show deviation. The measured photons arrive earlier than predicted by the diffusion approximation. The peaks of the theoretical (broken) computed curves are normalized to the peak of the experimental data, whereas the dash-dot curves are normalized to the total intensity of the experimental results. None of the theoretical plots from the diffusion approximation agrees with the experimental results when $z / l_t < 10$ [at early time].

The temporal distribution of photon for anisotropic scattering media and small z / l_t can differ significantly from the prediction of the diffusion approximation. To illustrate the point, the solid curve in Fig. 6.2(d), where $z / l_t = 2.8$, the photons are found to arrive substantiately earlier. These plots show that more photons arrive at early times. At later times $\approx 300\ ps$, the theoretical (dash-dot curve) and experimental curves merge.

A quantitative evaluation where the diffusion approximation breaks down is computed from the average time of photon arrival which is given by

$$\bar{t} = \int_0^\infty dt'\ t'\ I(t')\ /\ \int_0^\infty dt'\ I(t') \tag{6.3}$$

where $I(t')$ is the temporal distribution of the scattered pulse measured experimentally. The theoretical prediction of the average arrival time can be obtained exactly from eq. (6.1) as

$$\bar{t} = \frac{1}{2} \frac{z(z + 4z_0)}{v l_t} \quad . \tag{6.4}$$

The average time of arrival $\bar{t}$ as a function of z / l_t predicted by equation (6.4) is plotted by a solid curve in Fig. 6.4. The average time of arrival of the experimental results are computed from equation (6.3). The results from random media of bead diameters $d = 0.296, 0.46, 1.09, 3.134$ and $11.9\ \mu m$, are represented by plots of star, triangle, octagon, square and rose in Fig. 6.4. A dotted curve is plotted from eq. (6.4) times 0.9 to indicate where the experimental data deviates by more than 10%. The data displayed in Fig. 6.4 clearly demonstrates that the average time of arrival deviate by more than 10% occurs when $z / l_t \approx 10$. The deviation increases as z / l_t is reduced further below 10 and much more photons arrive earlier than predicted by diffusion theory. Anisotropic scattering as well as coherent interference

among the multiple scattered waves may account for the earlier arrival of the photons.

6.5 Conclusion

The temporal distribution of photon arrival after propagating through a slab of random medium of less than 10 transport mean free path thick cannot be predicted by diffusion approximation. The photons are found to arrive increasingly earlier as the optical thickness of the slab decreases. A better theoretical formulation is required which need to take the followings into account: (1) the finite particle size scatters the light in the forward direction and thus effectively reduces the time for the photons to transverse through the slab. (2) the possibility of coherent interference of the multiple scattered light which will result an earlier arrival of photon.

Chapter VII

Summary and Future directions

7.1 Summary

Time and angle resolved techniques are introduced as a versatile technique to study photon migration in random media. The phenomenon of weak photon localization is observed on the sub-picosecond time domain and in biological tissues. The measurement of the angular profiles of the coherent peak at various times after an incident pulse shows that the angular width of the coherent peak becomes narrower as the light propagating through a longer scattering path in the random medium. The temporal profile of a backscattered pulse can be characterized by the transport mean free path, the scattering mean free path, and the absorption length. The weak photon localization and the backscattered pulse are shown as a viable non-invasive technique to probe the optical properties of biological material and as a potential diagnostic tool in medicine.

The ultrafast laser pulse propagating through a slab of random medium is shown to consist of two components, the coherent and incoherent components. These two components have been angle and time resolved. The pulse profile and the direction of the coherent pulse remain unchanged. There is a substantial amount of temporal and angular broadening for the incoherent pulse. These broadening depend of the scatterer size and

concentration, and the thickness of the slab. The temporal profiles of the incoherent pulse were found to increasingly deviate from the diffusion approximation as the thickness of the random medium is decreased below 10 transport mean free path.

7.2 Future direction

This thesis work provides a small step forward on understanding light scattering and pulse propagation in random media. There is a lot more important work to be performed for theorist, experimentalist, and technologist to bring about a better understanding of light scattering in random medium and to find novel applications of light scattering. Some important work to be done are listed below.

7.2a Photon localization

Photon migration in random media is best studied from the temporal profile of the scattered pulse. Weak photon localization is due interference of the multiple scattered light and its time reversed counterpart. Strong photon localization is predicted to occur in a strongly scattering medium where the transport mean free path is less than the wavelength of the photon. The constructive interference among the multiple scattered light effectively reduces rate of photon migration through the random medium and the diffusion coefficient is reduced. This reduction of diffusion coefficient can be observed from the temporal profile of the scattered pulse. Thus time resolved technique should be used to investigate the phenomenon of photon localization. Studies should be concentrate on when and how the photon localization occurs, such as dependent of wavelength, size of the particle, and the size of

the medium.

The interference amount the multiple scattered light inside the random medium is suggested to be studied using two pulses separated at different time intervals. The interference between the multiple scattered light of the two pulses can be measured by the following steps. (1) Ultrafast laser pulses are separated into two beams by a beam splitter where one beam is delayed with respect to the other. These two beams traveling in the same direction and are incident simultaneously on a random medium. The transmitted intensity in time domain is recorded by a streak camera. (2) The first beam is blocked so that only the second beam is incident on the random medium and the transmitted intensity is measured. Then the second beam is blocked and the first beam is allowed to incident on the random medium. The two separately measured intensity is summed together, this total intensity do not contained the interference amount the multiple scattered light. (3) Thus, the intensity in (1) minus that in (2) will give us the interference between the two scattered pulse at a given time delay.

7.2b Pulse propagation

The propagation of an ultrafast laser pulse through a slab of random medium is a difficult theoretical problem and is yet to be solve. Our experimental results on the transmitted pulse profile cannot be described by presently available theory. These experimental results should provide a valuable insight for the theorist to find a suitable approximate solution for pulse propagation.

The velocity of the coherent pulse should be investigated both experimentally and theoretically.

7.2c Microscopic medium characterization

The gross optical properties of a random medium can be characterized by the transport mean free path and the absorption length from the angular and temporal profiles of the scattered pulse. The details of the fluctuation of dielectric constant in the medium is unknown, such as the position and the degree of randomness. The possibility of uniquely determine the microscopic details of the dielectric fluctuation from the temporal profile of the scattered pulse should be investigated.

Appendices

A1 Derivation of $|\vec{x}_i - \vec{x}_f| = \sqrt{l_t L / 3}$

Let $\vec{x}_i - \vec{x}_f = \bar{z}$ be the mean displacement of the photon after propagating through a path length of L in a random medium with transport mean free path l_t.

The probability that a photon transverses a distance z at time t in an infinite random medium may be approximated by diffusion theory

$$P(z,t) = \frac{1}{8(\pi Dt)^{3/2}} e^{-z^2/4Dt} \quad , \tag{a1.1}$$

where D is the diffusion coefficient. The time t can be related to the distance the photon propagate L by $L = vt$, where v is the speed of the photon in the random medium. Eqn. (a1.1) can be rewritten in term of L as

$$P(z,L/v) = \frac{1}{8(\pi DL/v)^{3/2}} e^{-z^2/4DL/v} \quad , \tag{a1.2}$$

The mean distance the photon transverses after propagating a distance L is

$$\bar{z} = \int_0^\infty dz \; zP(z,L) \; / \; \int_0^\infty dz \; P(z,L). \tag{a1.3}$$

$$= \sqrt{4 l_t L / 3\pi}$$

$$\approx \sqrt{l_t L / 3}$$

A2 Sample preparation

The random media consist of latex beads suspended in water. The latex bead samples were bought from Sigma Chemical and the original volume fraction of the latex bead is 10%. A lower concentration of latex bead medium is prepared by diluting the original 10% medium by adding deionized water.

v_s ml of the 10% volume fraction medium consists of $0.1v_s$ ml of latex beads. When v_w ml of water is added, the volume fraction f of the latex beads is

$$f = \frac{0.1v_s}{v_s + v_w} . \tag{a2.1}$$

If the diameter of the latex bead is d m, the number density of the latex bead is

$$n = \frac{0.1v_s}{(4/3)\pi(d/2)^3 (v_s + v_w)} m^{-3} . \tag{a2.2}$$

A3 Derive

$$\frac{I_c}{I_t} = \frac{1}{1+f\ (e^{z/l_s}-1)/\ (1+z/l_t)}$$

When light propagates through a slab of random medium with thickness z, the intensity of the coherent component of the scattered light is

$$I_c = I_0\, e^{-z/l_s} \tag{a3.1}$$

where I_0 is the incident light intensity and l_s is the scattering mean free path. The intensity of the incoherent or diffuse photon is

$$\begin{aligned} I_{inc} &= I_0 - I_c = I_c\ e^{z/l_s} - I_c \\ &= I_c\ (e^{z/l_s} - 1)\ , \end{aligned} \tag{a3.2}$$

where eq. (a3.1) has been used.

The probability for a diffuse photon to pass through a slab of random medium is similar to the gambling problem. Suppose a person starts with an initial capital C, the probability that he win an amount of W is

$$\begin{aligned} P &= \frac{C}{C+W} \\ &= \frac{1}{1+W/C}\ . \end{aligned} \tag{a3.3}$$

Photon propagation through a slab of random medium is a 1-dimensional problem. When a photon incident on a random medium, the mean position of the photon is at one transport mean free path deep inside the random medium. The probability of this photon to propagate through a distance z is similar to the above gambling problem and is given as

$$P = \frac{1}{1+az/l_t}\ , \tag{a3.4}$$

where a is on the order of unity. The intensity of the transmitted incoherent photon I_{tra} is the intensity of the incoherent photon (eq. a3.2) times the probability of this incoherent photon to pass through (eq. a3.4) and is given by

$$I_{tra} = Iinc \ P \tag{a3.5}$$

and

$$I_{tra} = \frac{I_c \ (e^{z/l_t} - 1)}{1+z/l_t} \ , \tag{a3.6}$$

where a is taken as 1. These transmitted incoherent photons is spread in all direction. On those photons scatter within a faction of solid angle f is measured by the detector. Thus, the measured transmitted incoherent intensity is $f\, I_{tra}$. The ratio of I_c to total measured transmitted intensity is

$$\frac{I_c}{I_t} = \frac{I_c}{I_c + f\, I_{tra}} \ , \tag{a3.7}$$

Substitute eq. (a3.6) into eq. (a3.7), one obtains

$$\frac{I_c}{I_t} = \frac{1}{1+f \ (e^{z/l_t}-1)/ \ (1+z/l_t)} \tag{a3.8}$$

Computer Programs

A5.1 To compute the temporal profile of the backscattered pulse using eq. (1.9) to (1.11)

```
# Input parameters :
#     sl       the transport mean free path
#     sal      the absorption length
#     w0       the FWHM of the streak camera response
#     theta    the angle of the backscattering
#     name     Output data file name
#
#  Output:
#     The temporal profile of the backscattered pulse
#
#
#     Program name :  weak/pul1.r
#     Computer program to compute the temporal profile of
#     the reflected pulse using eq. (2.9) to (2.11)
#
      dimension cj(300),tt(300),tp(100)
      External F
      common sl,sal,ti,w0,theta
      real sl,sal,ti,w0,theta
print*,"enter: transport mean free path & absorption length (micro)"
read*,sl,sal
print*,"enter: streak camera response (FWHM) and the angle of scattering "
read*,w0,theta
print*,"enter output filename"
read*,name
#
#     Input parameters for BQUAD
      EPS=.1
      ESREL=1.0E-2
      EPSAB=0.
#
#     Time axis from -20 to 200 ps
open(2,file=name)
```

```
      do it=1,220,1 {
      ti=float(it)-19.999     # time zero at 20
      tt(it)=ti
#
#     For the time response of the streak camera
      by convolution
do kk=1,40,1 {
tp(kk)=ti-19.0+(float(kk))-1.0
}
#
#     Integration subroutine
      CALL BQUAD(F,40,tp,EPS,cj(it),ERREST)
#
#     find the maximum for normalization
      if(cj(it).gt.cjmax) cjmax=cj(it)
      }
#
      do i=1,220 {
      cj(i)=cj(i)/cjmax
      time=tt(i)
      write(2,99) time,cj(i)
      }
 99   Format (2(F8.4,1x))
      stop
      end
#
#      u is parabolic cylindrical function
#      and p=(1/sqrt(2pi))exp(x**2/4)u(x)
      Function p(x)
      common sl,sal,ti,w0,theta
      real sl,sal,ti,w0,theta
      pi=3.14156
      s=sqrt(pi/8.)
      if (x.ge.3.) go to 32
      y1=(1.+x*x)*exp(x*x/4.)
      y2=x
      yy=x
      nmax=20
      do n=1,nmax {
      yy=yy*(2*n+2.)*x*x/(2.*n*(2.*n+1.))
      y2=y2+yy
      }
```

```
      p=(y1*s*exp(x*x/4)-y2)/(4.*s)
      go to 42
 32   nnmax=10
      ux=1.
      u1=1.
      do nn=1,nnmax {
      u1=-u1*(2.*nn+1.)*(2.*nn+2.)/((2**nn)*x*x)
      ux=ux+u1
      }
      p=ux/(4.*s*x**3)
 42   continue
      return
      end
#
#     Function to be integrated
      Function F(tp)
      common sl,sal,ti,w0,theta
      real sl,sal,ti,w0,theta
      pi=3.14156
      hw=2.
      x=(hw*sl*5.058*sin(theta))**2
      tpp=ti-tp
      time=tp
      tp1=150.*time/sl
      if (time<=0.0) FA=0.0
      else {
      tp1=sqrt(tp1)
      FA=p(tp1)*(1.+exp(-75.*time*x/sl))
      }
      F=20.*exp(-(tpp/w0)**2)*FA*exp(-225.*time/sal)
      return
      end
```

A5.2 Computer program to compute the angular profile of the backscattered light using eq. (1.8)

```
#  Input parameter:
#     sl       the transport mean free path
#     sal      the absorption length
#     w0       the angular FWHM of the detecting system
      name     output data file name
#
#  Output:
#     The angular profile for the backscattered light
#
#     Program name: /weak/weak.r
#     Computer program to compute the angular profile of
#     the backscattered light using eq. (2.8)
#
      dimension cj(150),tt(150),tp(30)
      External F
      common sl,sal,angle,w0
      real sl,sal,angle,w0
      character*8 name
      pi=3.14156
      w0=0.20e-3              # Angular resolution FWEM=2xw0
#     Input parameters for BQUAD
      EPS=.1
      ESREL=1.0E-2
      EPSAB=0.
print*,"enter scattering length & absorption length (micro)"
read*,sl,sal
print*,"enter output filename"
read*,name
open(2,file=name)
      do iang=1,150,1 {       # angular range
      angle=float(iang)/50000.0-0.00301
      tt(iang)=angle
do kk=1,30,1 {
tp(kk)=angle+(float(kk)-15.0)/20000.0     # resolution of detection
}
      CALL BQUAD(F,30,tp,EPS,cj(iang),ERREST)
# find the maximum for normalization
      }
```

```
cjmin=cj(1)
      do i=1,150 {
      cj(i)=cj(i)/cjmin
      angle=tt(i)
      write(2,99) angle,cj(i)
      }
      do i=150,1,-1 {
      angle=-tt(i)
      write(2,99) angle,cj(i)
      }
 99   Format (2(F10.6,1x))
      stop
      end
#     Function to be integrated
      Function F(tp)
      common sl,sal,angle,w0
      real sl,sal,angle,w0
pi=3.14156
tpp=angle-tp
pangle=abs(tp)
z0=0.7*sl
q=2.0*pi*pangle/0.465
qa=sqrt(3.0/(sl*sal))
q=sqrt(q**2+qa**2)
      FA1=(1.0-exp(-2.0*q*z0))/(q*sl)
      FA2=(1.0+q*sl)**2
      FA=(1.0+FA1)/FA2+2.0*z0/sl+1.0
      FR=exp(-(tpp/w0)**2)
      F=FA*FR
      return
      end
```

A5.3 To compute σ_s

```
#  Input parameter:
#     arad    radius of the bead (μm )
#     name    name for the output file
#
#  output:
#     σs  (10^-12 m^2)
#
#     program name :   mie/mie.r
#     Mie theory to calculate the exact scattering cross section
#     of spherical particle
      real*8 dda,ddb,sca,ext,bkr,bki,b1,rm,x,y,zetar(-1:300)
      real*8 zetai(-1:300),A(0:300),ca(300),cb(300),dar(300),dai(300)
      real*8 ar(300),ai(300),dbr(300),dbi(300),br(300),bi(300)
      character*10 name
b1=13.51       # 2*pi/lambda(=0.465micro)
rm=1.193       # relative refractive index of the latex beads in water
      print*,"enter output file name"
      read*,name
      open(1,file=name)
do i=1,8,1 {   # 8 input radii to be calculated
      print*,"enter the radius of the particle in micro"
      read*,arad
      x=b1*arad    # 2*pi*radius/lambda
      y=rm*x
zetar(-1)=dcos(x)
zetai(-1)=0.0-dsin(x)
zetar(0)=dsin(x)
zetai(0)=dcos(x)
A(0)=dcos(y)/dsin(y)
sca=0.0
ext=0.0
bkr=0.0
bki=0.0
do n=1,300,1 {
      zetar(n)=(2.0*float(n)-1.0)/x*zetar(n-1)-zetar(n-2)
      zetai(n)=(2.0*float(n)-1.0)/x*zetai(n-1)-zetai(n-2)
      A(n)=0.0-float(n)/y+1.0/(float(n)/y-A(n-1))
      ca(n)=A(n)/rm + float(n)/x
      cb(n)=A(n)*rm + float(n)/x
```

```
      dar(n)=ca(n)*zetar(n)-zetar(n-1)
      dai(n)=ca(n)*zetai(n)-zetai(n-1)
dda=(dar(n)**2+dai(n)**2)
kk=n-1
if (dda>=1.0d35) break
      ar(n)=(ca(n)*zetar(n)-zetar(n-1))*dar(n)/dda
      ai(n)=0.0-(ca(n)*zetar(n)-zetar(n-1))*dai(n)/dda
      dbr(n)=cb(n)*zetar(n)-zetar(n-1)
      dbi(n)=cb(n)*zetai(n)-zetai(n-1)
ddb=(dbr(n)**2+dbi(n)**2)
if (ddb>=1.0d35) break
      br(n)=(cb(n)*zetar(n)-zetar(n-1))*dbr(n)/ddb
      bi(n)=-(cb(n)*zetar(n)-zetar(n-1))*dbi(n)/ddb
      }
do ii=kk,1,-1 {
# compute the total scattering cross section
sca= sca+(2.0*float(ii)+1.0)*(ar(ii)**2+ai(ii)**2+br(ii)**2+bi(ii)**2)
# compute the scattering cross section
ext= ext+(2.0*float(ii)+1.0)*(ar(ii)+br(ii))
# compute the scattering cross section
bkr= bkr+(float(ii)+0.5)*(-0.1)**n*(ar(ii)-br(ii))
bki= bki+(float(ii)+0.5)*(-0.1)**n*(ai(ii)-bi(ii))
}
sc=2.0*sca/x**2*(3.1416*arad**2)
ex=2.0*ext/x**2*(3.1416*arad**2)
bk=4.0*(bkr**2+bki**2)/x**2*(3.1416*arad**2)
rad=arad
      print*, x,sc
      write(1,*) rad,sc
}
      stop
      end
```

A5.4 To compute σ_s / σ_m

```
#  Input parameter:
#     arad     radius of the bead (μm )
#     name1          name for the output file
#
#  output:
#     σs / σm
#
#     program name :   mie/mie.r
#     Mie theory to calculate the exact scattering cross section
#    Mie theory to calculate the ratio of
#    scattering to momentum exchange scattering cross section
#    of spherical beads with different radii
character*10 name1
real ctheta(61)
real rm,x,y
common rm,x,y
External F1,F2
b1=13.61       # 2*pi/lambda(=0.465micro)
rm=1.193       # rm=1.193  relative refractive index of the latex beads in water
pi=3.13156
       print*,"enter output file name for sigma s and m"
       read*,name1
       open(1,file=name1)
do i=1,10,1 {                  # can compute up to 10 radii
       print*,"enter accuracy of int. EPS"
       read*,EPS
 print*,"enter the radius of the particle in micro"
 read*,arad
x=b1*arad     # 2*pi*radius/lambda
y=rm*x
#
# compute scattering cross section
#
do k=1,61,1 {
ctheta(k)=-1.0+(2.0/60.0)*(float(k)-1)
}
       CALL BQUAD(F1,61,ctheta,EPS,sigmas,ERREST)
#
# compute momentum-exchange scattering cross section
#
```

```
      CALL BQUAD(F2,61,ctheta,EPS,sigmam,ERREST)
ratio=sigmas/sigmam
      write(1,99) arad,ratio
}
99   Format (2(F10.4,1x))
stop
end
#
#      Function to be integrated
#
      Function F1(ctheta)
#
real rm,x,y
common rm,x,y
      F1=SQ(ctheta)
      return
      end
#
#      Function to be integrated
#
      Function F2(ctheta)
#
real rm,x,y
common rm,x,y
      F2=(SQ(ctheta))*(1.0-ctheta)
      return
      end
#
#compute the scattering amplitude A1**2
#
Function SQ(ctheta)
#
real dda,ddb
real A(0:300),wr(-1:300),wi(-1:300),p(-1:300),t(-1:300)
real ca(300),cb(300),dar(300),dai(300),ar(300),ai(300)
real dbr(300),dbi(300),br(300),bi(300)
real ctheta,angle
real rm,x,y
common rm,x,y
      angle=acos(ctheta)
      p(0)=0.0
      p(1)=1.0
```

```
      p(2)=3.0*ctheta
      t(0)=0.0
      t(1)=ctheta
      t(2)=3.0*cos(2.0*angle)
      wr(-1)=cos(x)
      wi(-1)=0.0-sin(x)
      wr(0)=sin(x)
      wi(0)=0.0-cos(x)
      A(0)=cos(y)/sin(y)
      s=(sin(angle))**2
do n=1,300,1 {
xn=float(n)
#
# compute a(n) and b(n)
#
      wr(n)=((2.0*xn-1.0)/x)*wr(n-1)-wr(n-2)
      wi(n)=((2.0*xn-1.0)/x)*wi(n-1)-wi(n-2)
      A(n)=0.0-xn/y+1.0/(xn/y-A(n-1))
#
# compute a(n)
#
      ca(n)=A(n)/rm + xn/x
      dar(n)=ca(n)*wr(n)-wr(n-1)
      dai(n)=ca(n)*wi(n)-wi(n-1)
dda=(dar(n)**2+dai(n)**2)
kk=n-1
if (dda>=1.0d35) break
      ar(n)=(ca(n)*wr(n)-wr(n-1))*dar(n)/dda
      ai(n)=0.0-(ca(n)*wr(n)-wr(n-1))*dai(n)/dda
#
# compute b(n)
#
      cb(n)=A(n)*rm + xn/x
      dbr(n)=cb(n)*wr(n)-wr(n-1)
      dbi(n)=cb(n)*wi(n)-wi(n-1)
ddb=(dbr(n)**2+dbi(n)**2)
if (ddb>=1.0d35) break
      br(n)=(cb(n)*wr(n)-wr(n-1))*dbr(n)/ddb
      bi(n)=-(cb(n)*wr(n)-wr(n-1))*dbi(n)/ddb
#
# compute pi(n) and tau(n) at a given angle
#
```

```
if(n<=2) next
p(n)=ctheta*((2*xn-1.)/(xn-1.0))*p(n-1)-p(n-2)/(xn-1.0)
t(n)=ctheta*(p(n)-p(n-2))-(2.*xn-1.)*s*p(n-1)+t(n-2)
}
AR1=0.0
AI1=0.0
AR2=0.0
AI2=0.0
do n=kk,1,-1 {
xn=float(n)
fa1=(2.*xn+1.0)/(xn*(xn+1.0))
AR1=AR1+fa1*(ar(n)*p(n)+br(n)*t(n))
AI1=AI1+fa1*(ai(n)*p(n)+bi(n)*t(n))
AR2=AR2+fa1*(br(n)*p(n)+ar(n)*t(n))
AI2=AI2+fa1*(bi(n)*p(n)+ai(n)*t(n))
}
SQA1=AR1**2+AI1**2
SQA2=AR2**2+AI2**2
SQ=SQA1+SQA2
      return
      end
```

A5.5 Computer program to compute the temporal profile of the transmitted pulse from diffusion theory

```
#  Input parameter :
#     z       thickness of the random media
#     tmfp the transport mean free path
#     name3          name of the output file
#
#  Output:
#     Temporal profile of the transmitted pulse
#
#     Program name: /diff/lax1.r
#     The profile depends on:
#     Computer program to compute the temporal profile of
#     the transmitted pulse
#
      real cj(1600)
      character*10 name3
#     print*,"  thickness of the slab (m) ? "
      read*, z
      print*,"  transport mean free path tmfp (m) ? "
      read*, tmfp
      print*, " file name "
      read*,name3
      open(3,file=name3)
# parameters
z0=0.71*tmfp  # for boundary condition
d=z+2.*z0
pi=3.141593
theta=z*pi/d
dif=(7.5e-5)*tmfp  # diffusion coefficient =v1/3 (ps-1)
do i=4,1200,2 {
t=float(i)          # t  time (ps)
      sum=0.0
      do m=100,1,-1 {
      fm=float(m)
      ff=(pi*fm/d)**2*(dif*t)
      term=fm*theta**2*sin(fm*theta)*exp(-ff)
      sum=sum+term
      }
cj(i)=sum
```

```
if(cj(i).gt.cjmax) cjmax=cj(i)
}
      fact=cjmax
      do i=4,1200,2 {
      time=float(i)
      cj(i)=cj(i)/cjmax
      write(3,99) time,cj(i)
      }
99    format(f6.0,1x,f10.5)
      stop
      end
```

A5.6 Computer program to compute the temporal profile of the transmitted pulse using Ishimaru formulation

```
#
#  Input parameters :
#     tb      time, start
#     te      time, end
#     ti      time, interval
#     scat    z / l_s
#     acc     accuracy of integration
#     wr      2αv / z
#     xr      integration variable
#     name    output file name
#
#  Output :
#     The temporal profile of the transmitted pulse
#
#     This program compute the pulse propagation through a random medium
#     using Ishimaru formulation
#
External F
double precision x(100),t,wr,tte,F,result,scat
real r1,r2
common scat,t,tte,acc,wr
character*10 name
#
#     Set the output unit to 'jout'
jout=I1MACH(2)
#
print*,"enter time begin, end, interval"
read*,tb,te,ti
print*,"enter scattering strength"
read*,scat
print*," accuracy"
read*,acc
print*," enter wr"
read*,wr
print*,"enter integration range"
read*,xr
x(1)=xr
print*,"enter filename"
```

```
read*,name
open(jout,file=name)
do i=2,99,1 {
x(i)=xr*(100.-float(i))/100.0
}
x(100)=1.d-6
do t=tb,te,ti {
call dbquad(F,100,x,acc,result,error)
#
r1=t
r2=0.0-result
write (jout,*) r1,r2
}
stop
end
#
double precision function F(x)
double precision x,wr,t,tte,A,B,C,F,scat
common scat,t,tte,acc,wr
#      compute the integral
A=dexp(-scat*(1.0-(datan(x))/x))
B=scat/2.0*dlog(1.0+x*x)/x
C=dexp(-0.274*x**2)
C=1
F=C*A*dcos(B-wr*x*t)
return
end
```

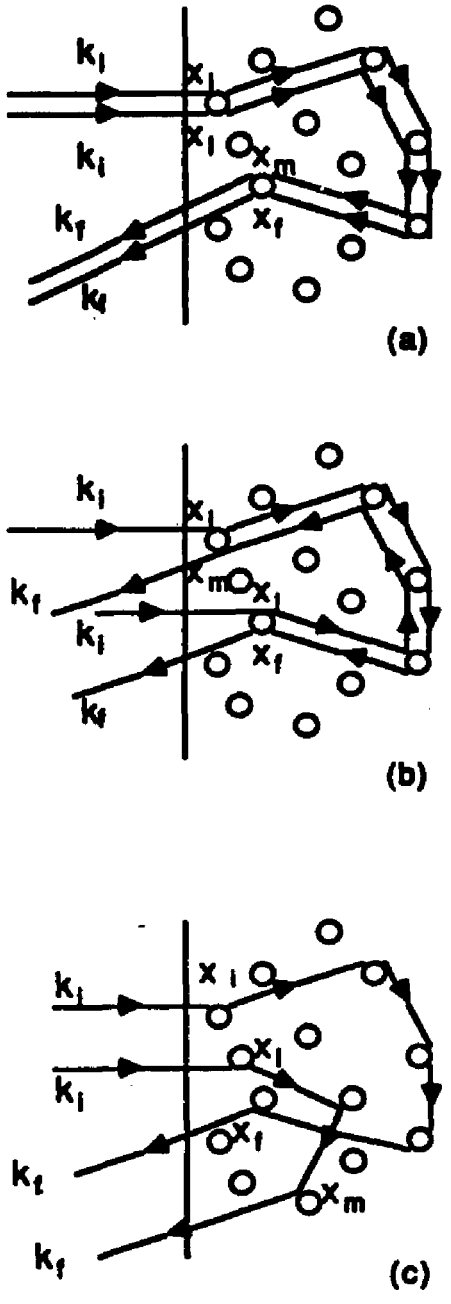

Fig.1.1 Light scattering through a series of scatterers. (a) $x_i = x_l$; $x_j = x_m$ (b) $x_i = x_m$; $x_j = x_l$ (c) others

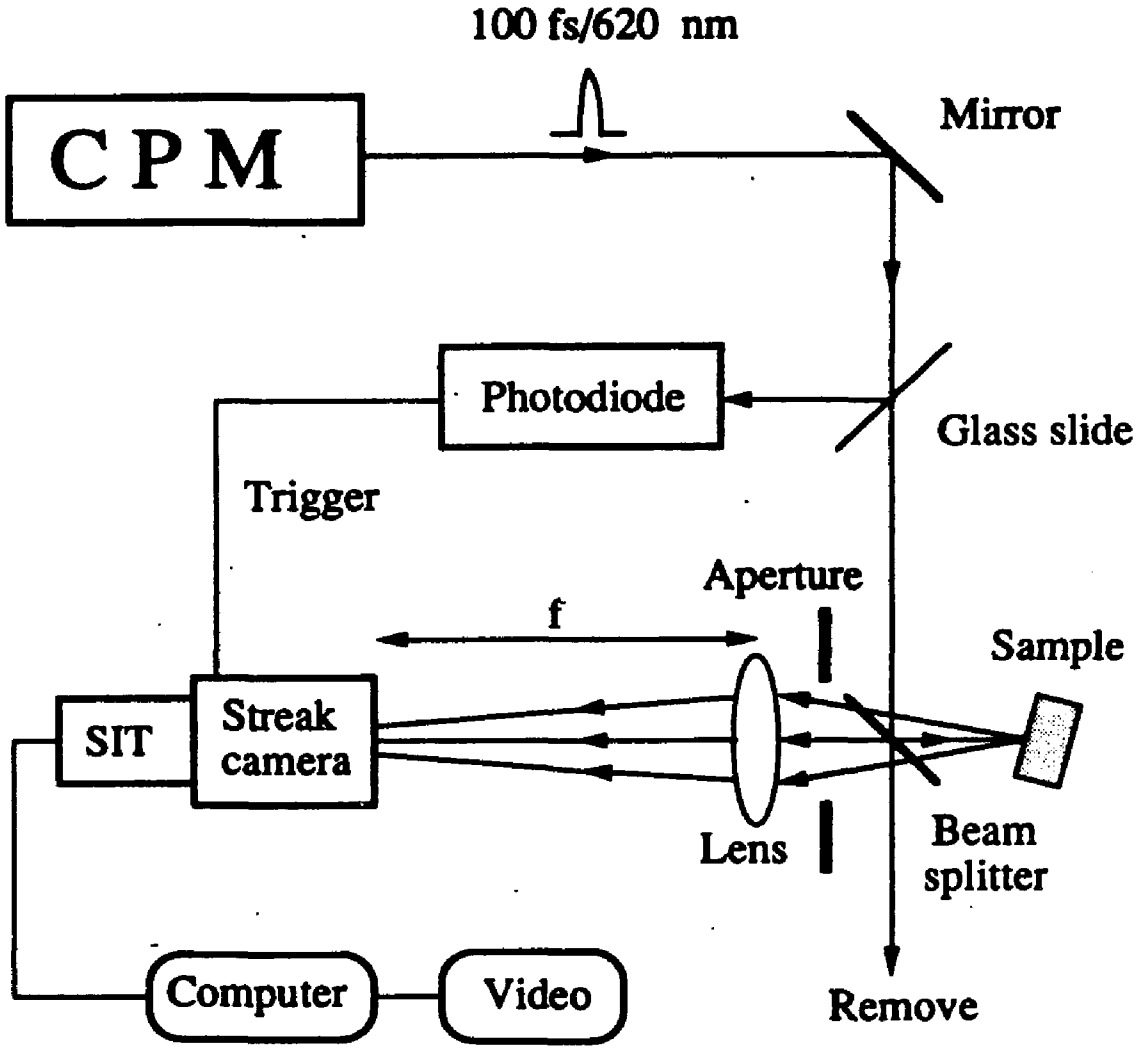

Fig.1.2 Experimental setup.

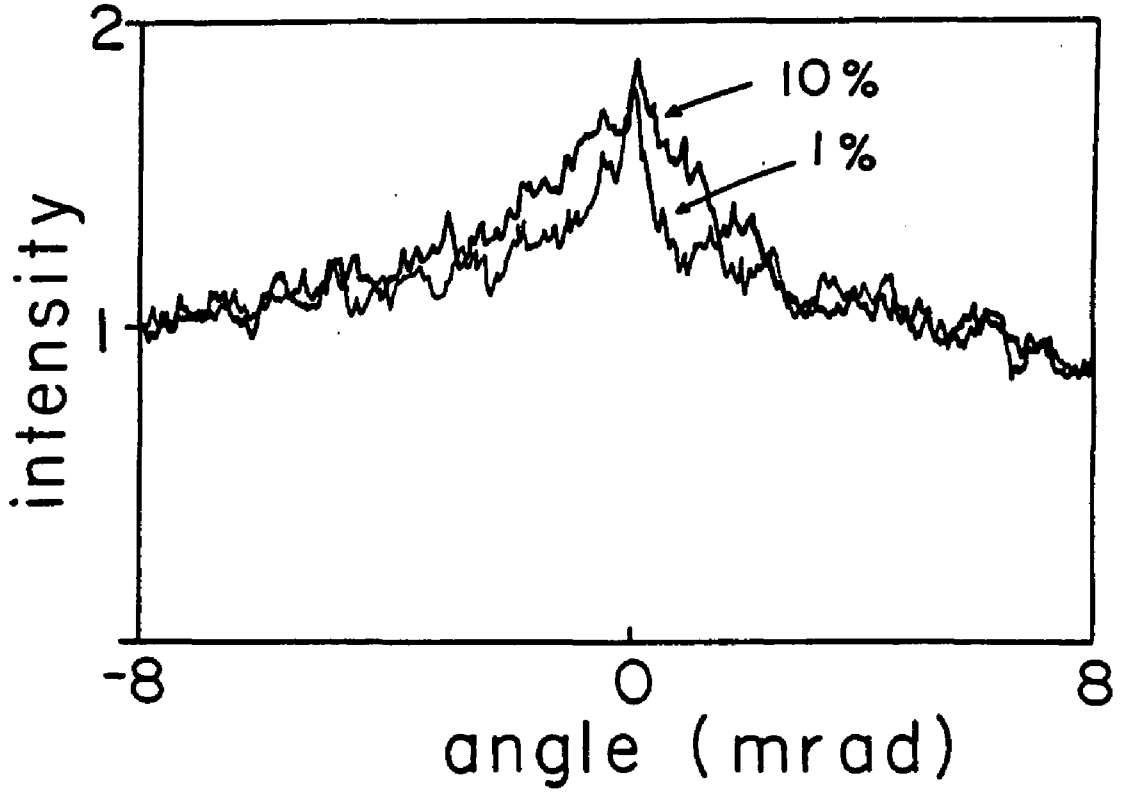

Fig.1.3 Intensity of scattered light from an incident femtosecond pulse as a function of scattering angle. Polystyrene sphere with diameter d=0.32μm suspended in water at two different concentrations; (a) 10% (b) 1%

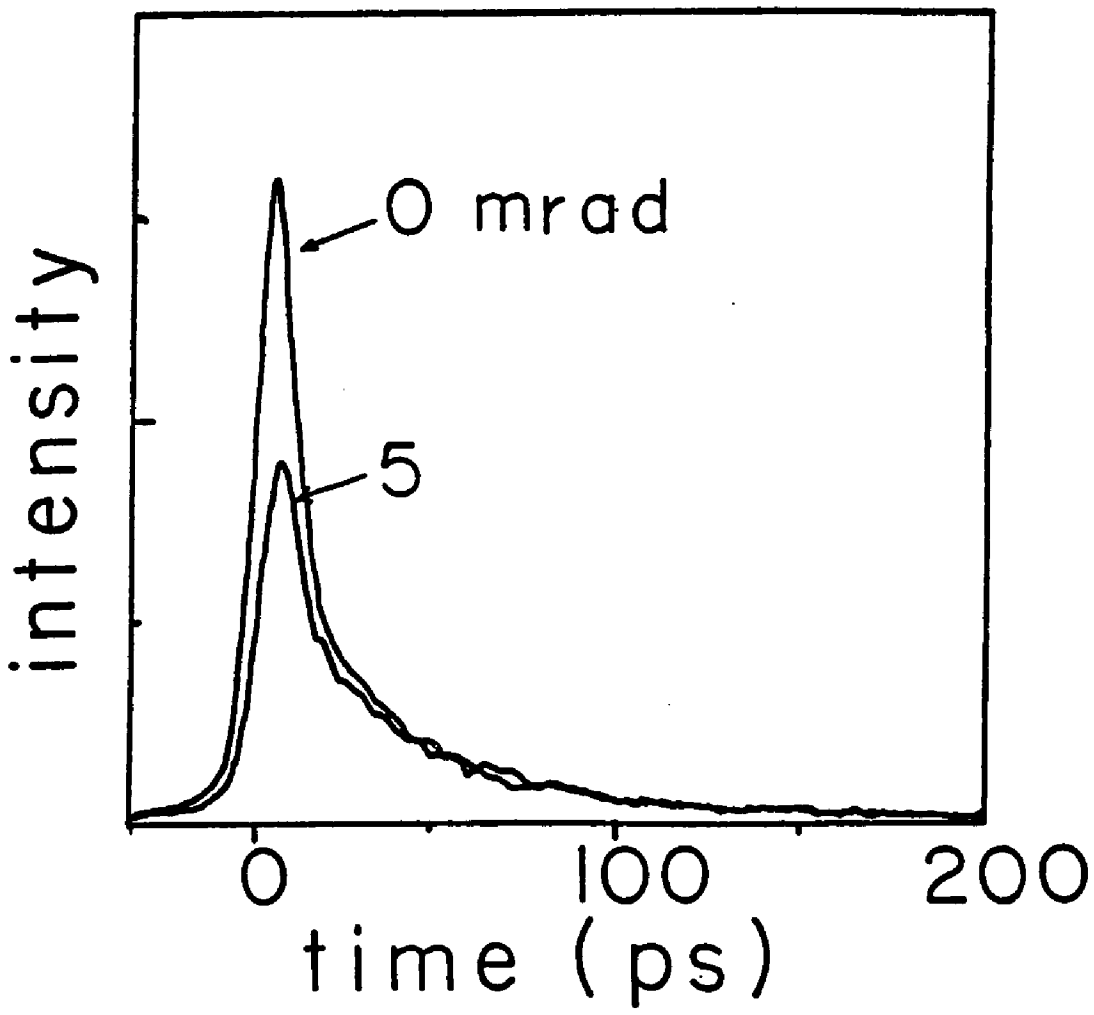

Fig.1.4 Intensity of backscattered pulses at two angles from 80fs pulses incident on a semi-infinite medium which has 1% volume concentration of latex beads of 0.33 μm diameter suspended in water; curve (a) 0.0 $\pm$0.2 mrad, curve (b) 5.0 $\pm$0.2 mrad.

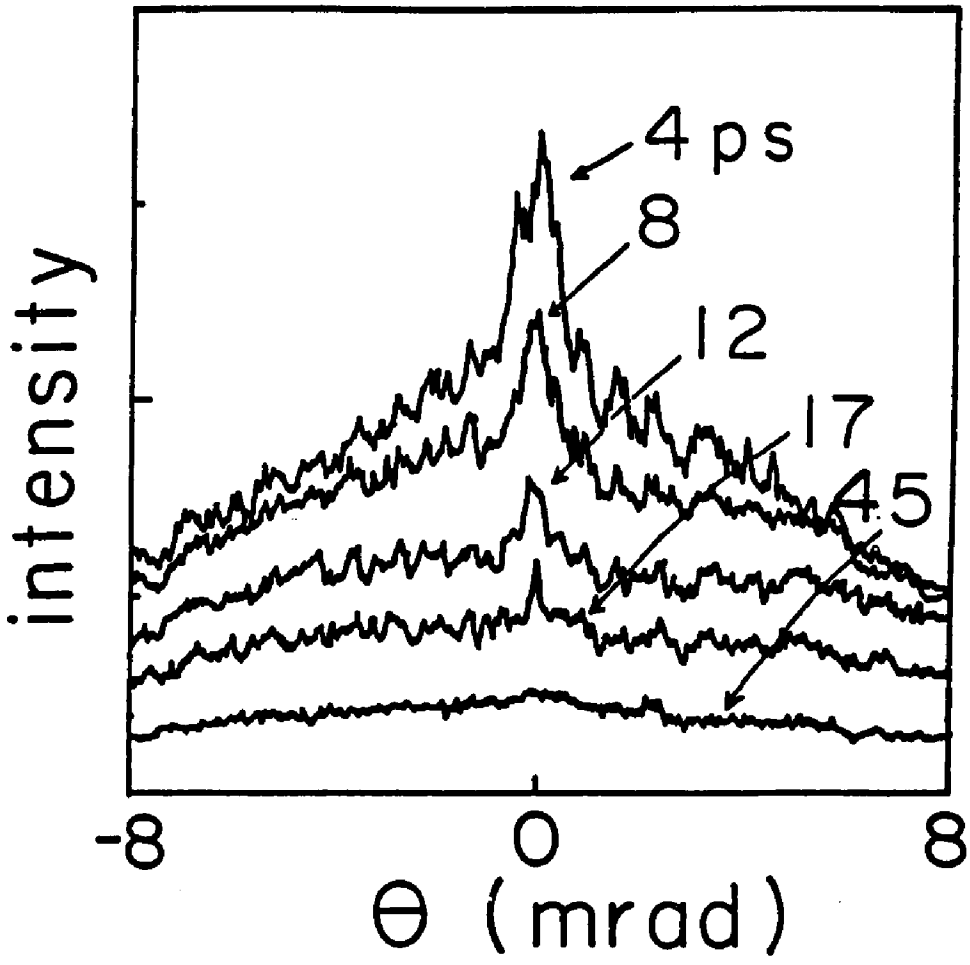

Fig.1.5 The line shape of backscattered light from a semi-infinite random medium which consist of a 1% volume concentration of latex beads with 0.33 μm diameter at various times after a 80fs incident pulse enter the medium: 4ps, 8ps, 12ps, 17ps, and 45ps which correspond to scattering pathlengths of 900, 1800, 2700, 3800, and 10,000 μm, respectively.

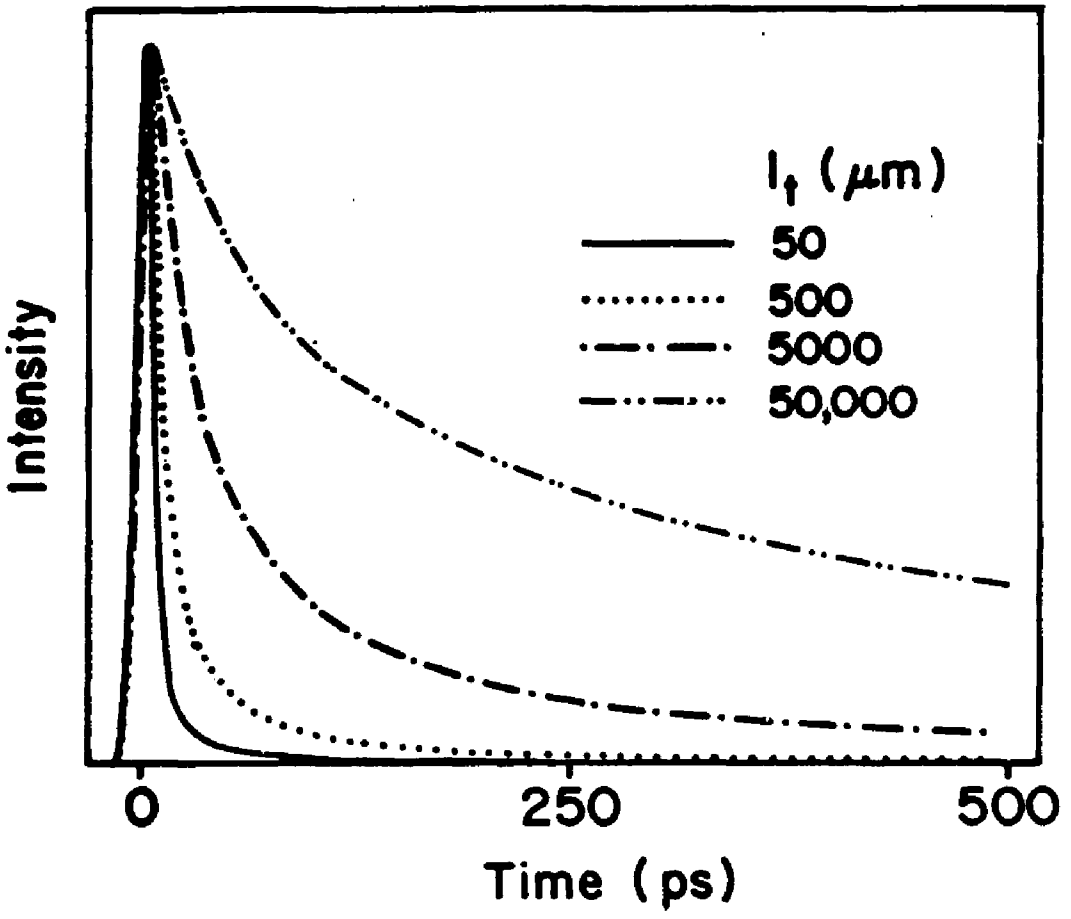

Fig.2.1 Temporal profiles of the backscattered pulses computed from eq. (1.11) with convolution of 8ps impulse response function for various values of l_t = 50, 500, 5000, and 50000μm .

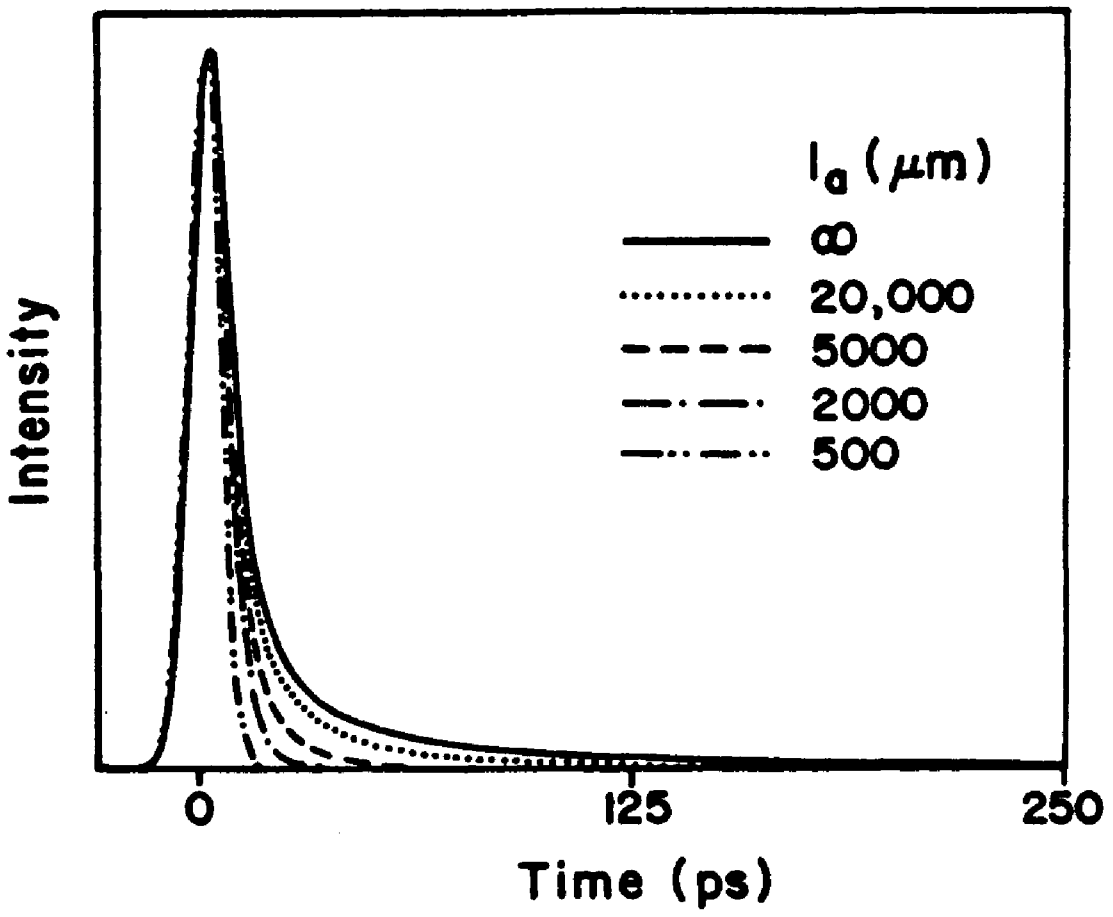

Fig.2.2 Temporal profiles of the backscattered pulse computed from eq. (2.11) with convolution of 8ps impulse response function for various values of l_a = ∞, 20000, 5000, 2000, and 500μm , given that l_t = 200μm .

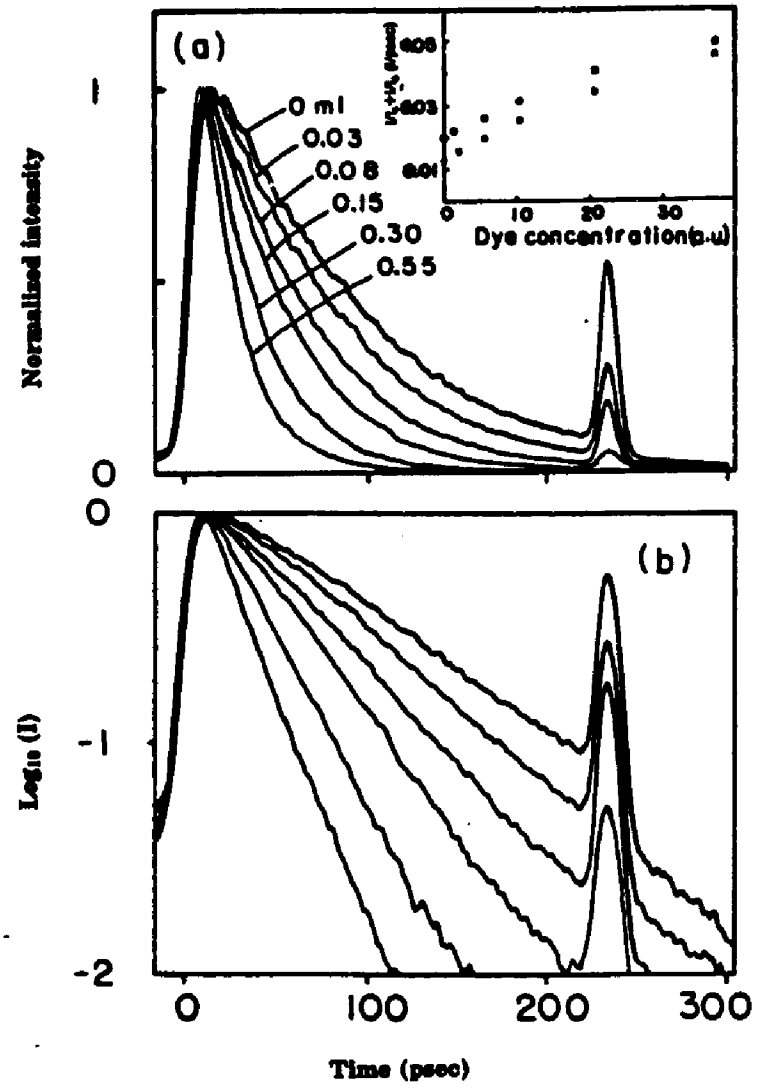

Fig.2.3 (a) Normalized backscattered intensity of femtosecond pulses incident upon a random medium with various volumes of dye added to the medium as indicated on the curves. The medium is 14.15 ml of a 0.106% solid fraction of 0.091 μm diameter latex beads suspended in water. The inset is a plot of $v(1/l_s + 1/l_a)$ versus concentrations of dye added to the medium: crosses, the medium is 14.15 ml of a 0.106% solid fraction of 0.091 μm diameter latex beads suspended in water; squares, the medium is 14.11ml of a 0.076% solid fraction of 11.9 μm diameter of latex beads suspended in water. (b) Semilog plots of the profile in (a).

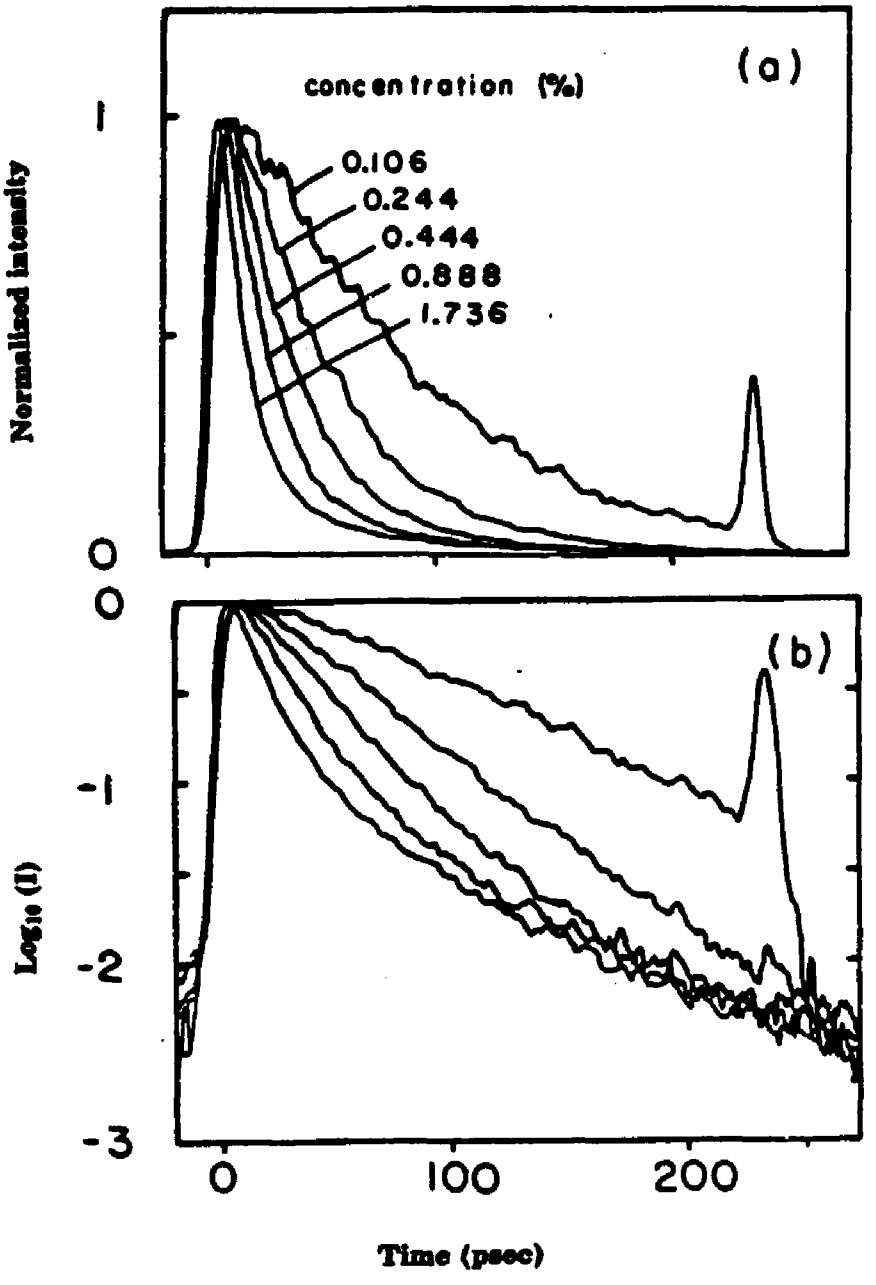

Fig.2.4 (a) Normalized backscattered pulse intensity from random media consisting of latex beads of 0.091 μm diameter suspended in water at various bead concentrations as indicated on the curves. (b) Semi-log plots of the profiles in (a).

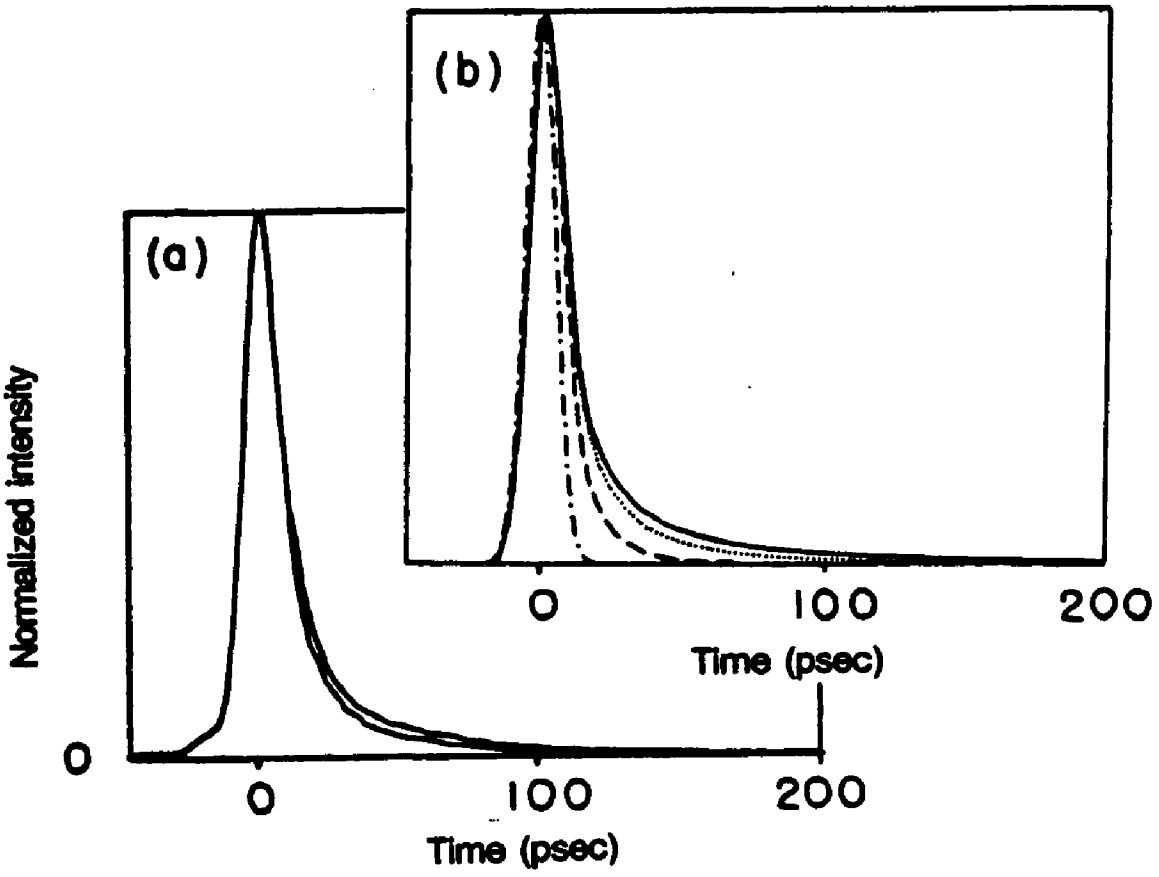

Fig.2.5 (a) Backscattered pulse profiles from a 0.91% concentration of latex beads of 0.49μm diameter suspended in water, with and without dye added into the medium. (b) Backscattered pulse profiles computed from eq. (1.11) that are best fits to the experimental results in Fig. (a). $l_t = 260\mu m$ and $l_a = 80\times10^3\mu m$ (no dye) and $20\times10^3\mu m$ (with dye) for the solid and dotted curves, respectively. The dashed and dashed-dotted curves are for strongly absorbing media with $l_a = 5\times10^3$ and $0.5\times10^3\ \mu m$, respectively.

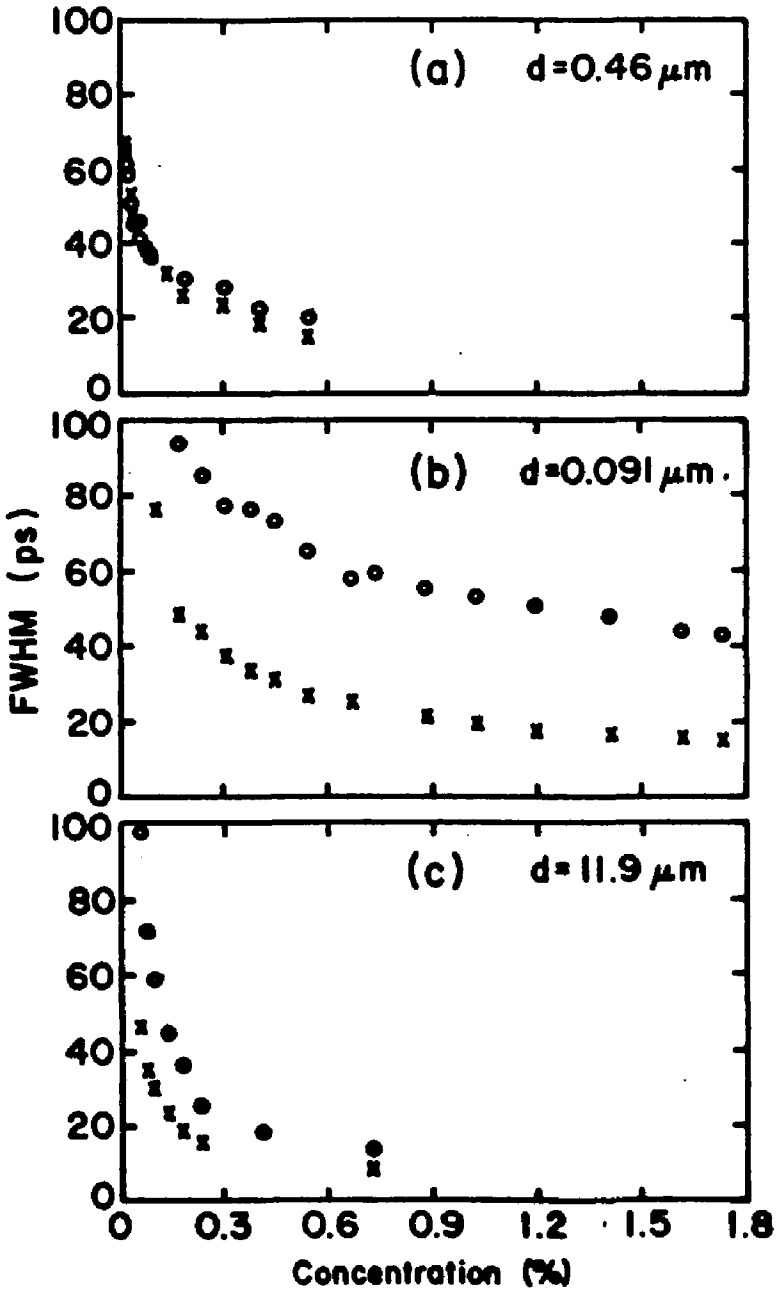

Fig.3.1 Plots of the full pulse width at half maxima (FWHM) of the back-scattered pulse versus concentration of latex beads suspended in water. Square curve: perpendicular polarization; and star curve: parallel polarization. The diameter of the latex beads are: (a) 0.46, (b) 0.091, and (c) 11.9μm .

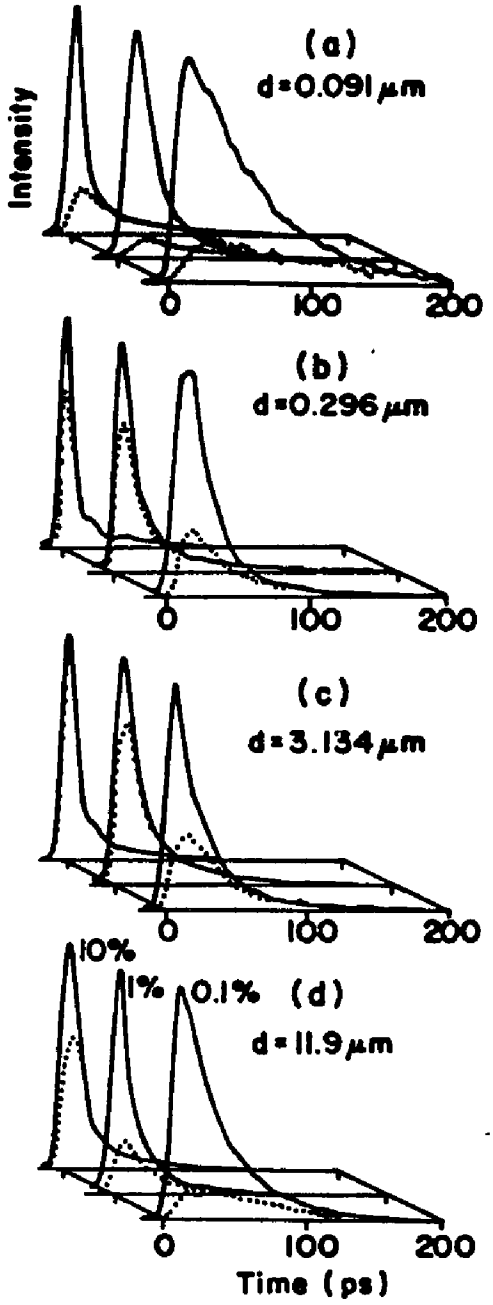

Fig.3.2 Temporal profiles for parallel (solid curves) and perpendicular (dotted curves) polarization components of the backscattered pulse from random media with different concentrations of 10%, 1%, and 0.1%, for diameters of: (a) 0.091, (b) 0.296, (c) 3.134, and (d) 11.9μm. The uncertainty in intensity is within 10%.

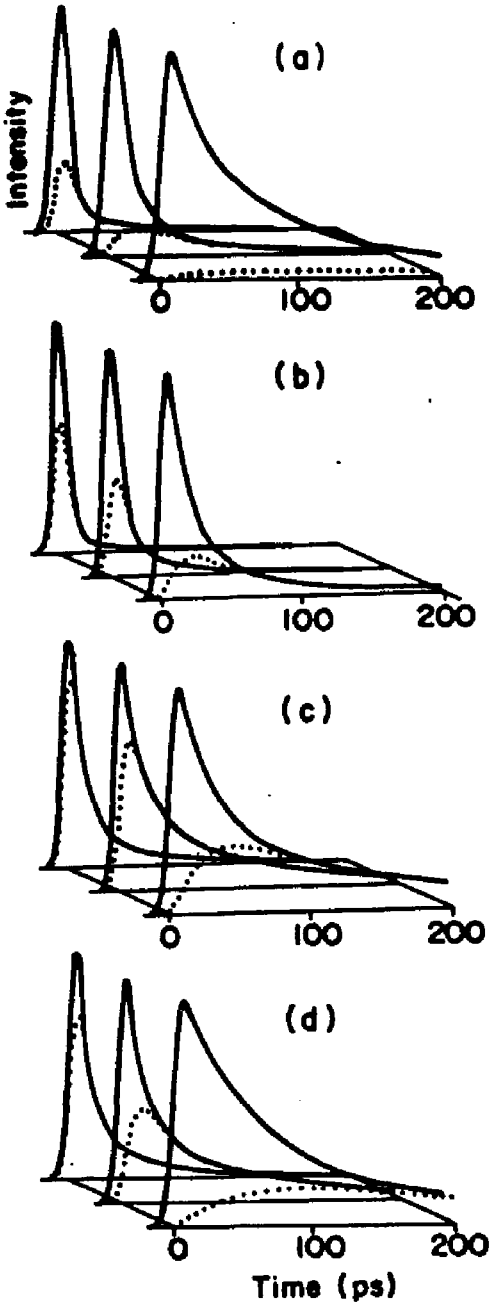

Fig.3.3 Computed curves from equations (1) to (5) for the corresponding experimental conditions displayed in Fig. 2. The values of these parameters: l and l_s computed from Mie theory are equal to: (a) 120, 113, (b) 23, 9, (c) 330, 12, and (d) 500 (estimated from the experimental curve), 36μm, respectively. The pathlength for 1% and 0.1% media increase by a factor of 10 and 100, respectively.

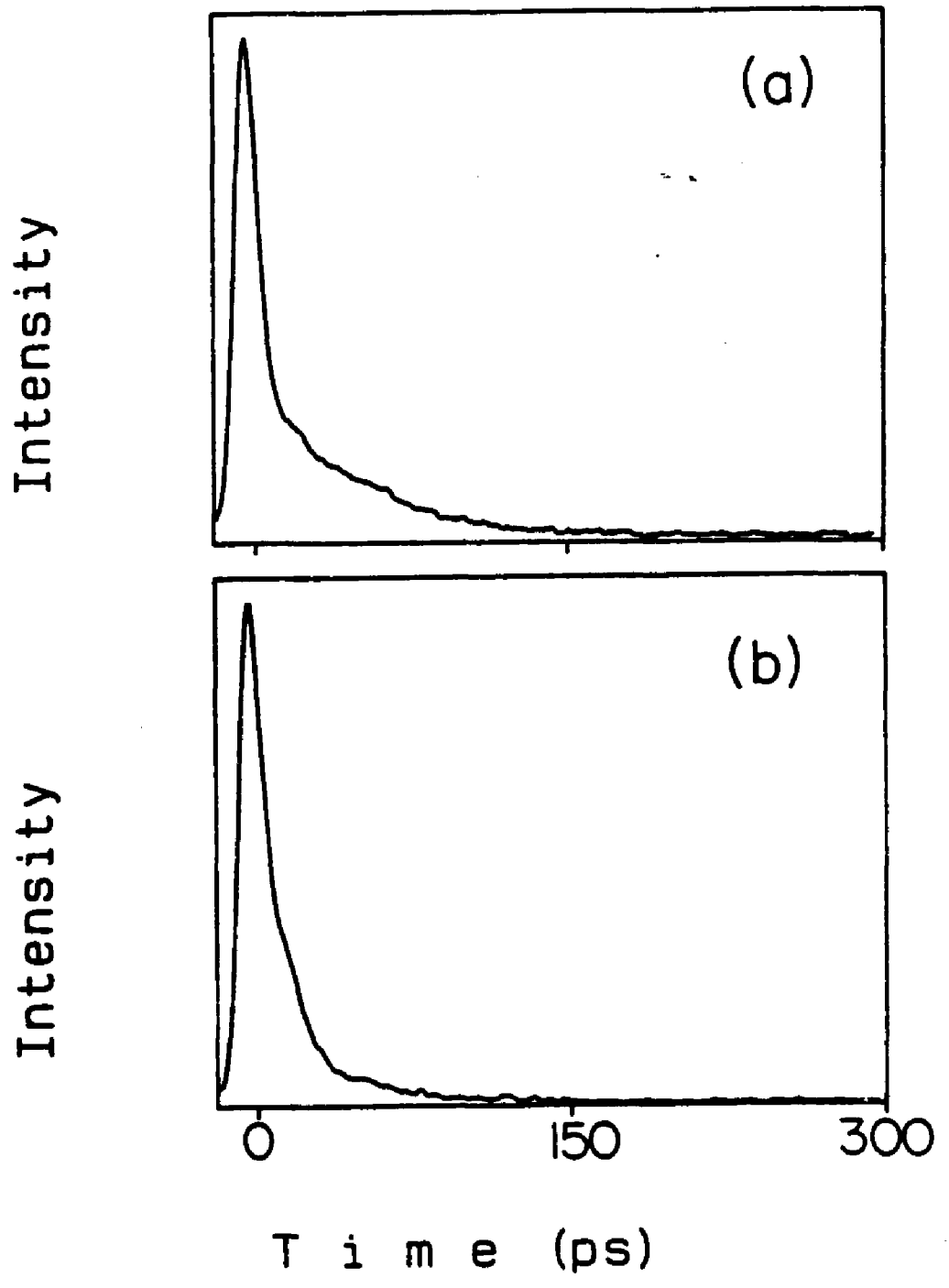

Fig.4.1 Temporal profiles of backscattered pulses from (a) fatty, and (b) muscle tissue of a heart.

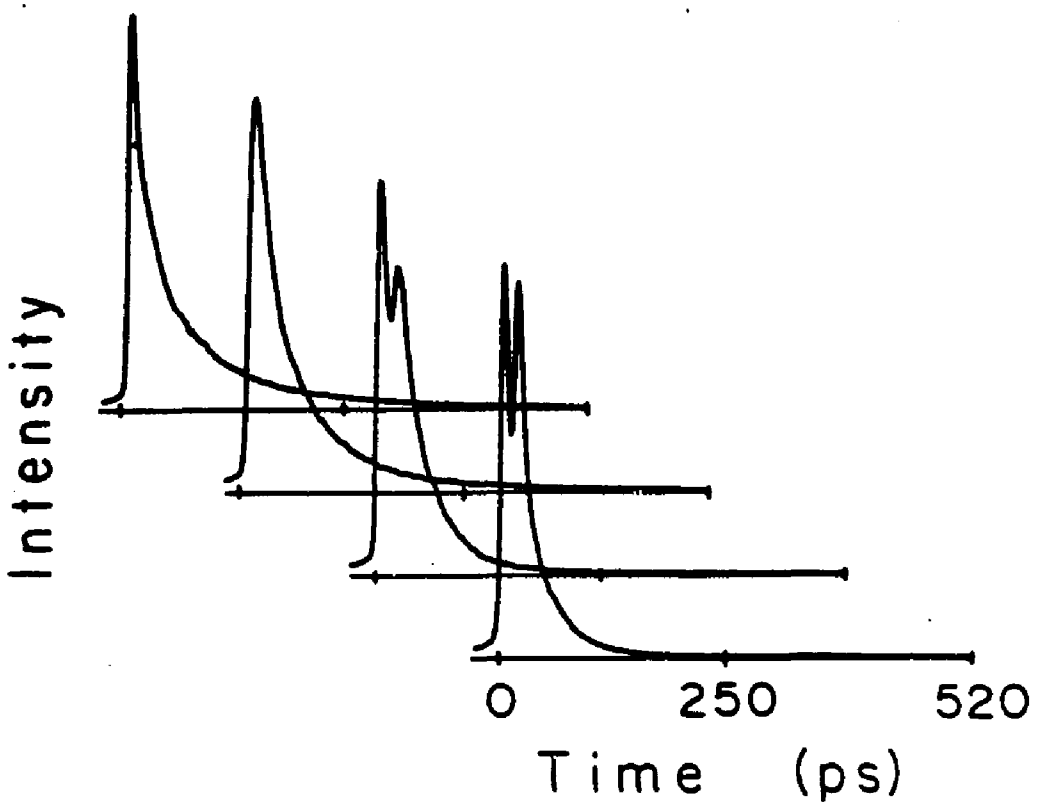

Fig.4.2 Temporal profiles of backscattered pulses from different portion of a tooth.

Fig.4.3 Angular profiles of backscattered pulses from a tooth.

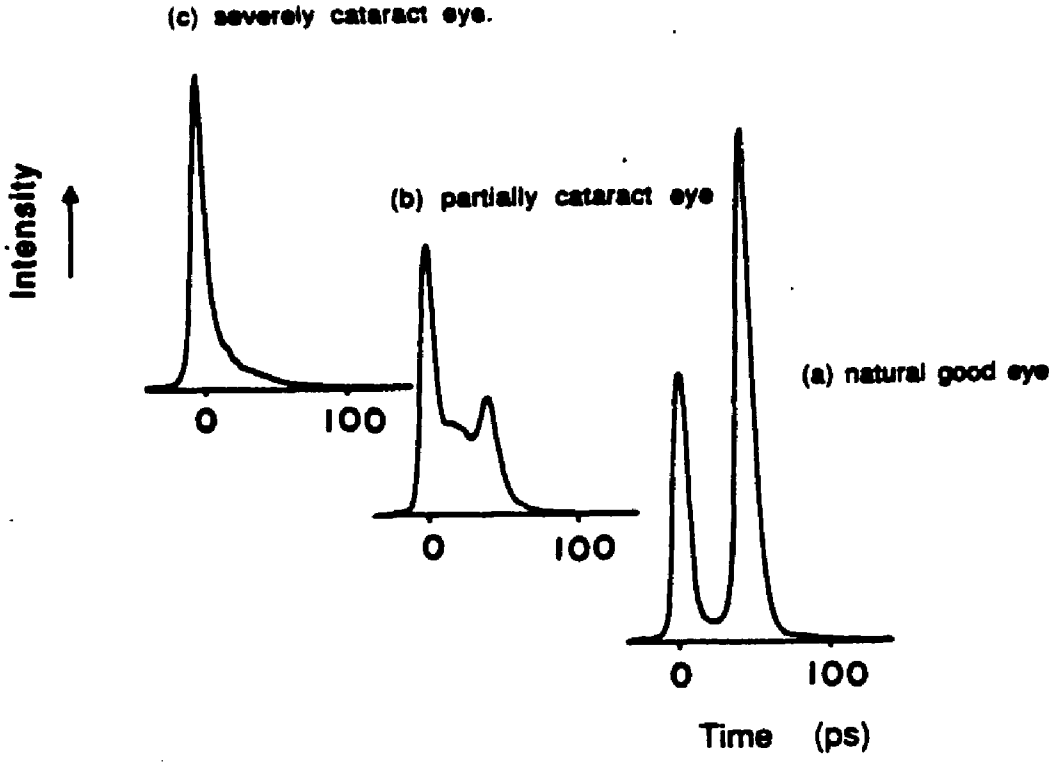

Fig.4.4 Temporal profiles of backscattered pulses from an eye with different characteristics. (a) good eye, (b) partially cataract eye, and (c) severely cataract eye.

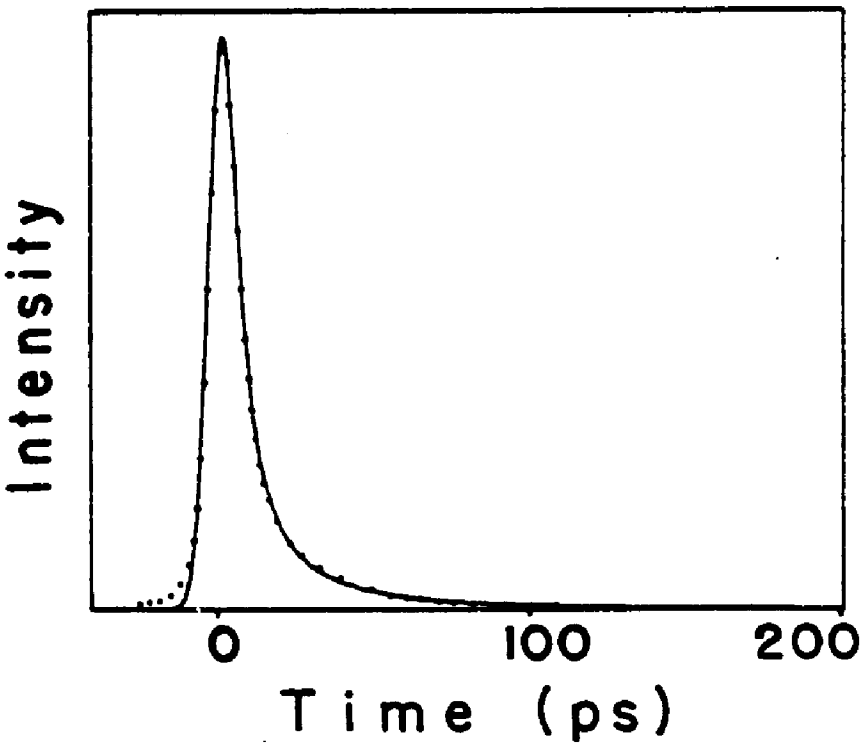

Fig.4.5 Fitting of the theory (solid curve) to the experimental data (dotted curve) for severely cataract eye.

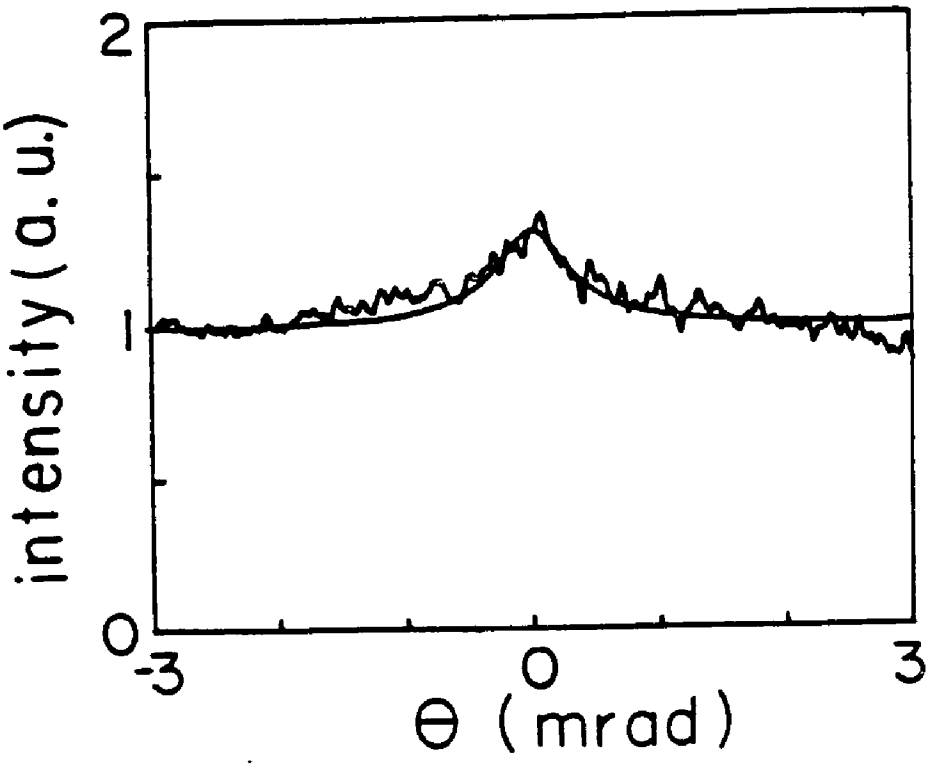

Fig.4.6 Angular distribution of intensity of light backscattered from human normal breast tissue. Solid curve is the theoretical fit from equation (1).

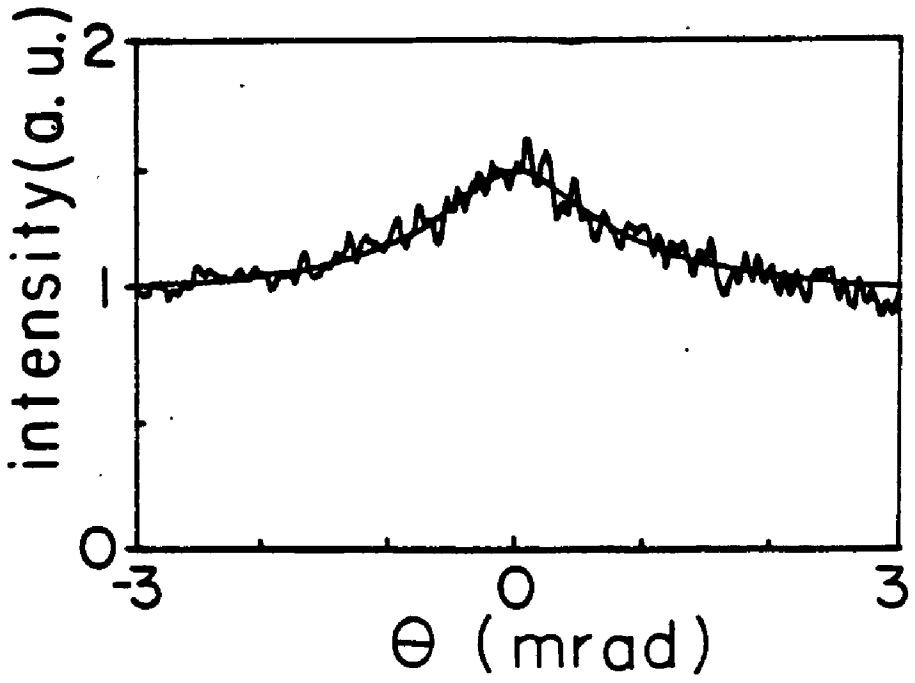

Fig.4.7 Angular distribution of intensity of light backscattered from human benign lung tissue. Solid curve is the theoretical fit from equation (1).

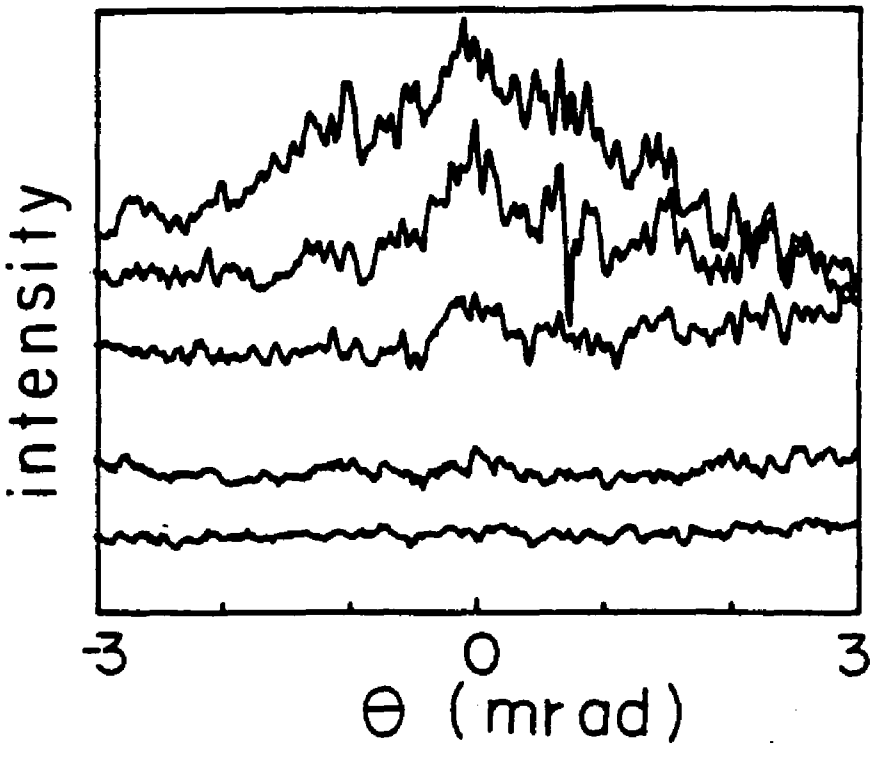

Fig.4.8 Intensity and the line shape of the coherent peak of the scattered light at various times after the 100fs pulse incident on lung cancer tissue. The selected time segments for the curves from the top are: 4, 8, 13, 22, and 35 ps.

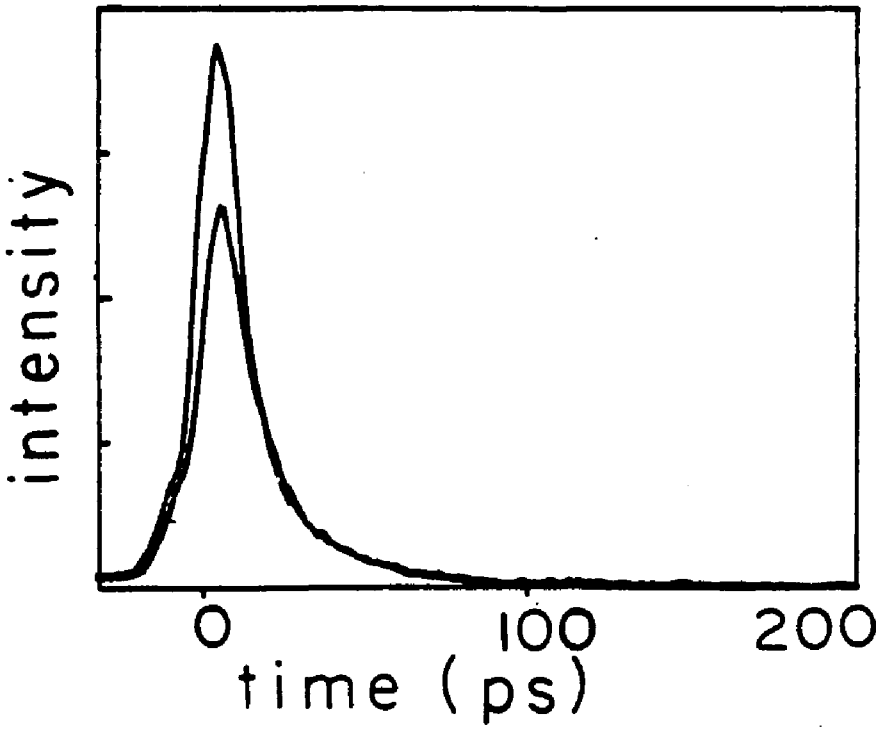

Fig.4.9 The temporal profiles of the backscattered pulse from lung cancer tissue. The higher curve is for light scattered at 0 mrad and the lower one is at 3 mrad.

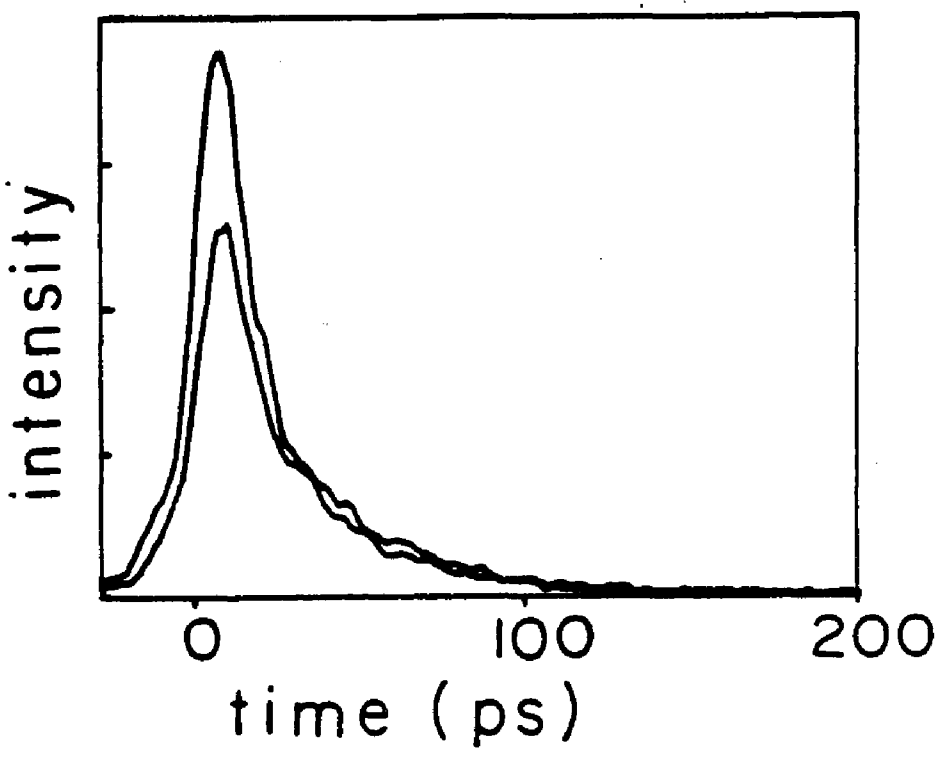

Fig.4.10 The temporal profiles of the scattered pulse from breast cancer tissue. The higher curve is for light scattered at 0mrad and the lower one is at 3mrad.

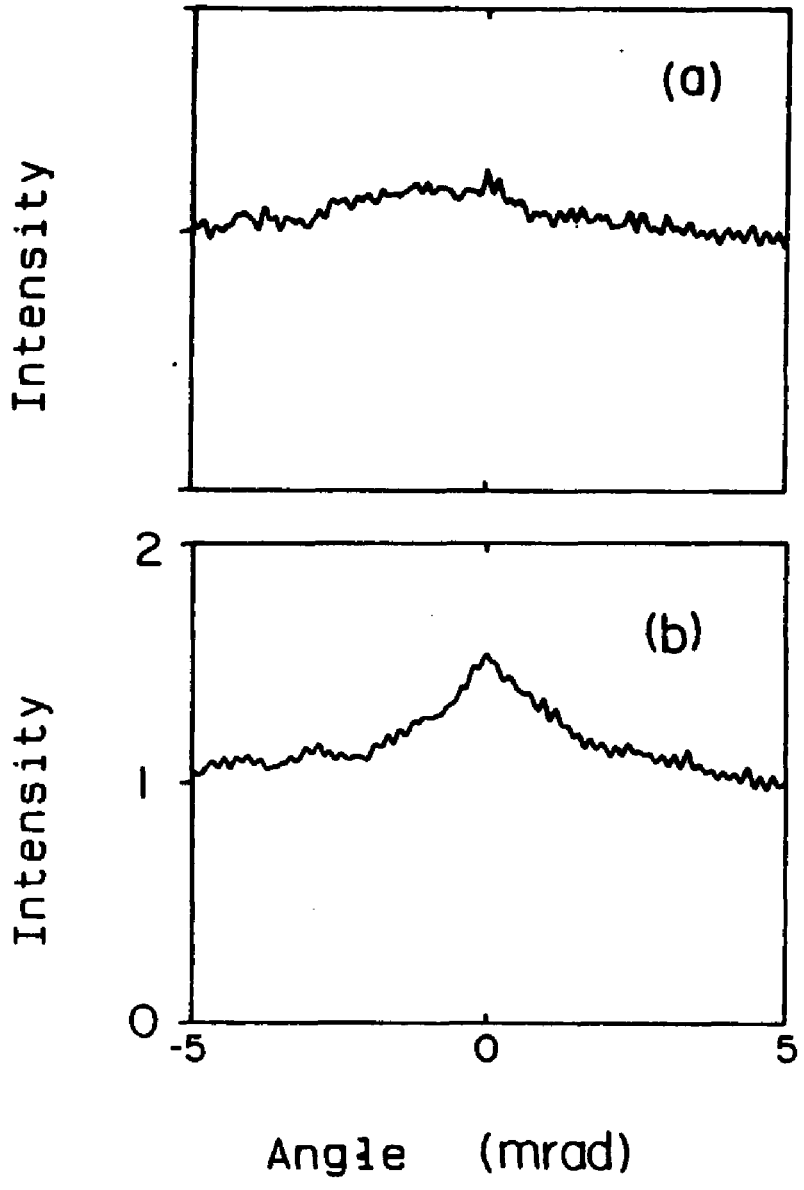

Fig.4.11 Angular profiles of backscattered pulses from a leaf: (a) a green leaf, (b) Leaf with chlorophyll extracted.

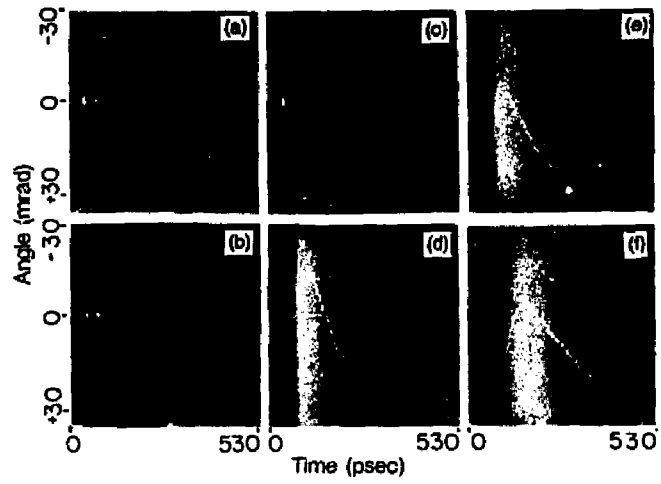

Fig.5.1 Photographs taken by a streak camera showing the angular and temporal behavior of light pulses propagating through a $10mm$ slab of random media. The first white spot is the reference pulse, the second spot is the coherent pulse, and the incoherent pulse is spread over a wide angular and temporal region. The curves trace the intensity versus time for waves scattered in the forward direction $\pm 4mrad$. The series of photographs are for an increasing number particle density for latex beads of $0.33\,\mu m$ diameter: (a) $n = 7.0\times10^{16}m^{-3}$, (b) $7.9\times10^{16}m^{-3}$, (c) $8.9\times10^{16}m^{-3}$, (d) $9.5\times10^{16}m^{-3}$, (e) $10.4\times10^{16}m^{-3}$, and (f) $17.3\times10^{16}m^{-3}$.

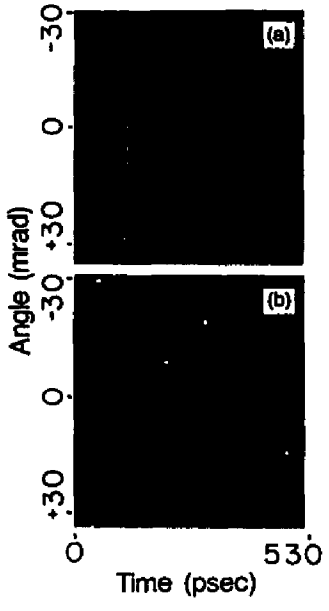

Fig.5.2 Photographs for scattered light through 10*mm* of random media in the intermediate scattering regime: (a) d=15.8 μm , $n\ \sigma_s\ z = 19.8$; (b) d=3.134 μm , $n\ \sigma_s\ z = 12.9$.

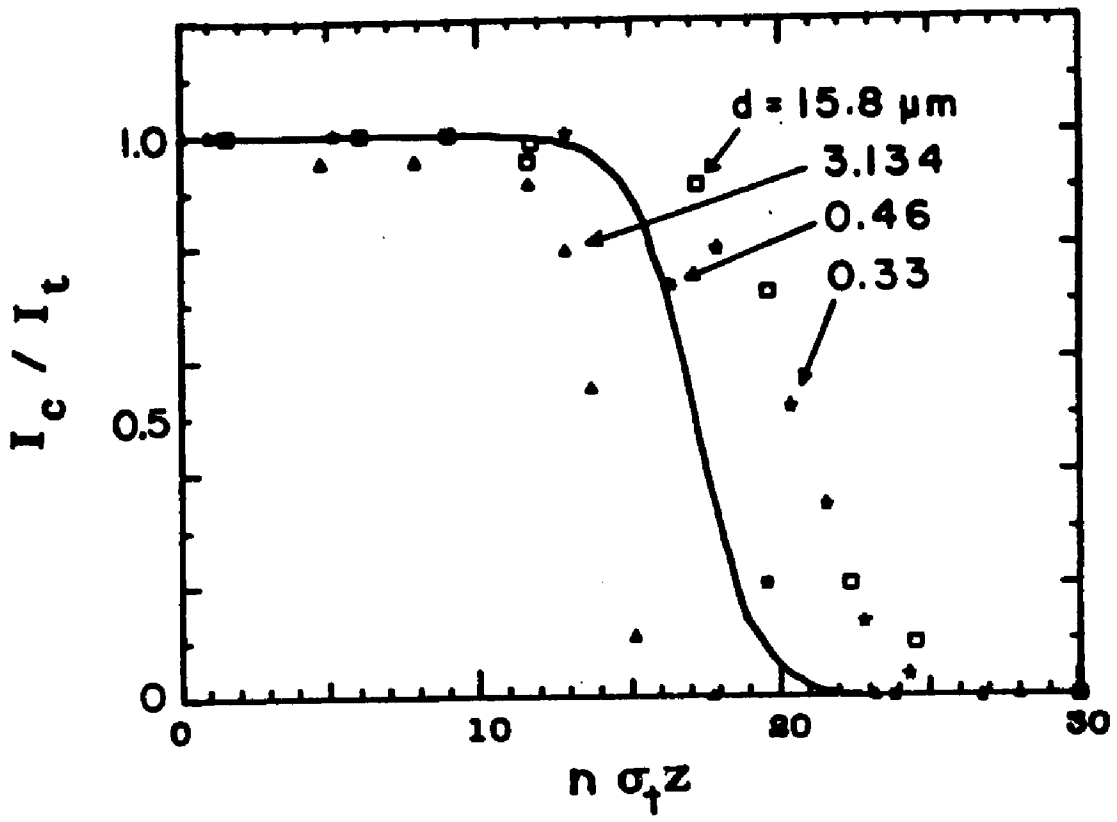

Fig.5.3 Plots of the ratio of coherent (I_c) to total (I_t) intensity of scattered light in the forward direction versus $n \sigma_s z$ for four different scatterer diameters. The solid curve is plotted from eq. (5.1), for bead diameter of $0.46\mu m$, where $\sigma_s = 0.109\times10^{-12} m^2$, $\sigma_m = 0.11\sigma_s$, and $f = 10^{-7}$.

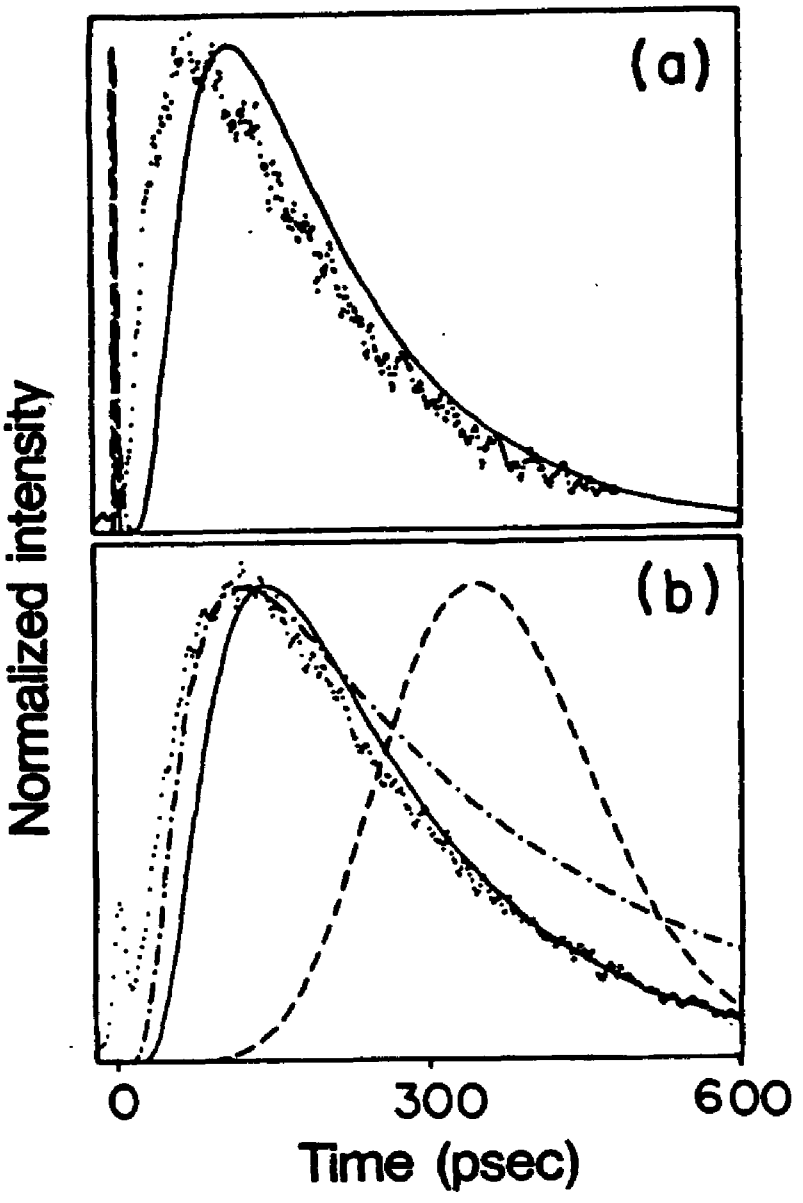

Fig.5.4 Normalized intensity of forward scattered light as a function of arrival time: (a) $d = 3.134\mu m$, $n\ \sigma_s\ z = 42.6$, and $l_t = 1.52mm$; (b) $d = 0.296\mu m$, $n\ \sigma_s\ z = 33.5$, and $l_t = 1.1mm$. Dotted curves, experimental result; solid curves, eq. (5.2); dashed curves, eq. (5.4); dashed-dotted curves, eq. (5.7).

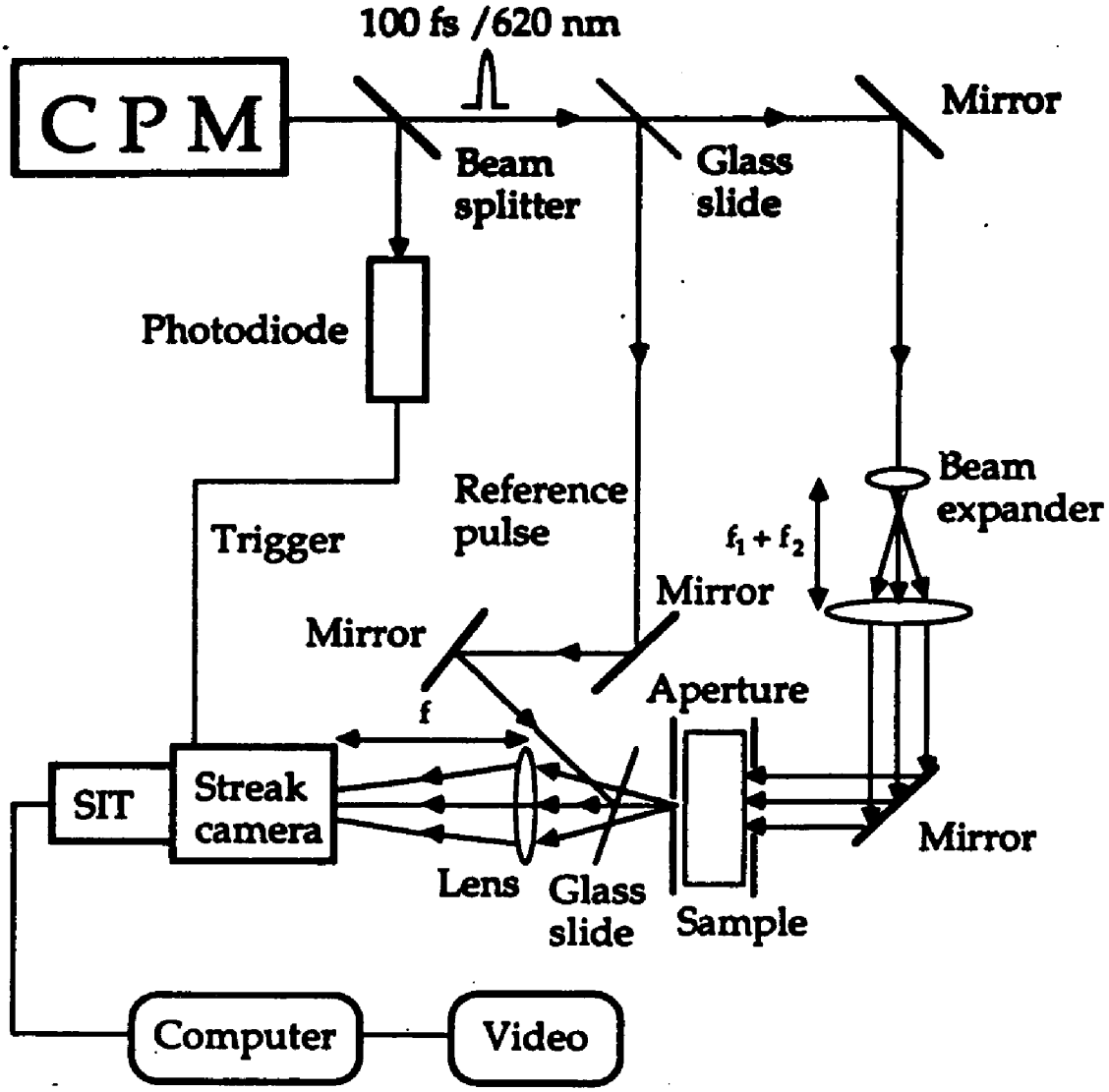

Fig.6.1 Schematic of experimental setup.

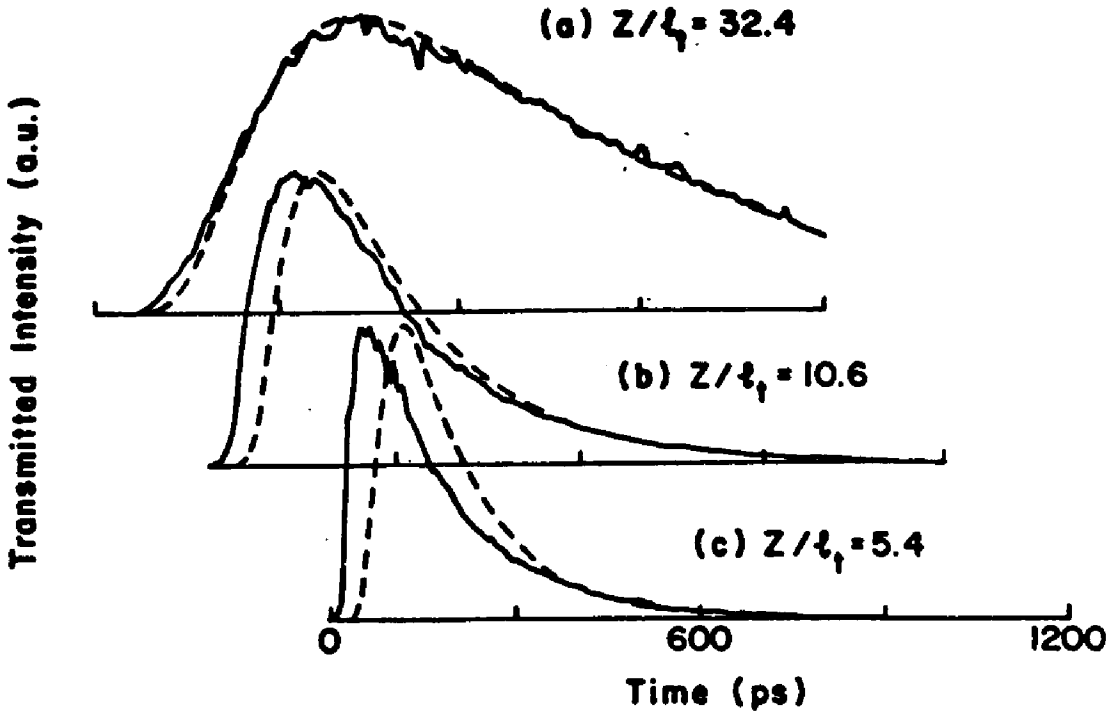

Fig.6.2 Transmitted pulse profiles of $10mm$ thick random media consisting latex beads of $0.296\mu m$ diameter. The bead concentrations n, l_t and z / l_t are: (a) $6.65\times10^{8}mm^{-3}$, $0.309mm$ and 32.4 ; (b) $2.18\times10^{8}mm^{-3}$, $0.941mm$ and 10.6 ; and (c) $1.10\times10^{8}mm^{-3}$, $1.853mm$ and 5.4; respectively. l_t is computed from equation (2). Solid curves are the experimental results and broken curves are computed from the diffusion theory where their peak intensity is normalized.

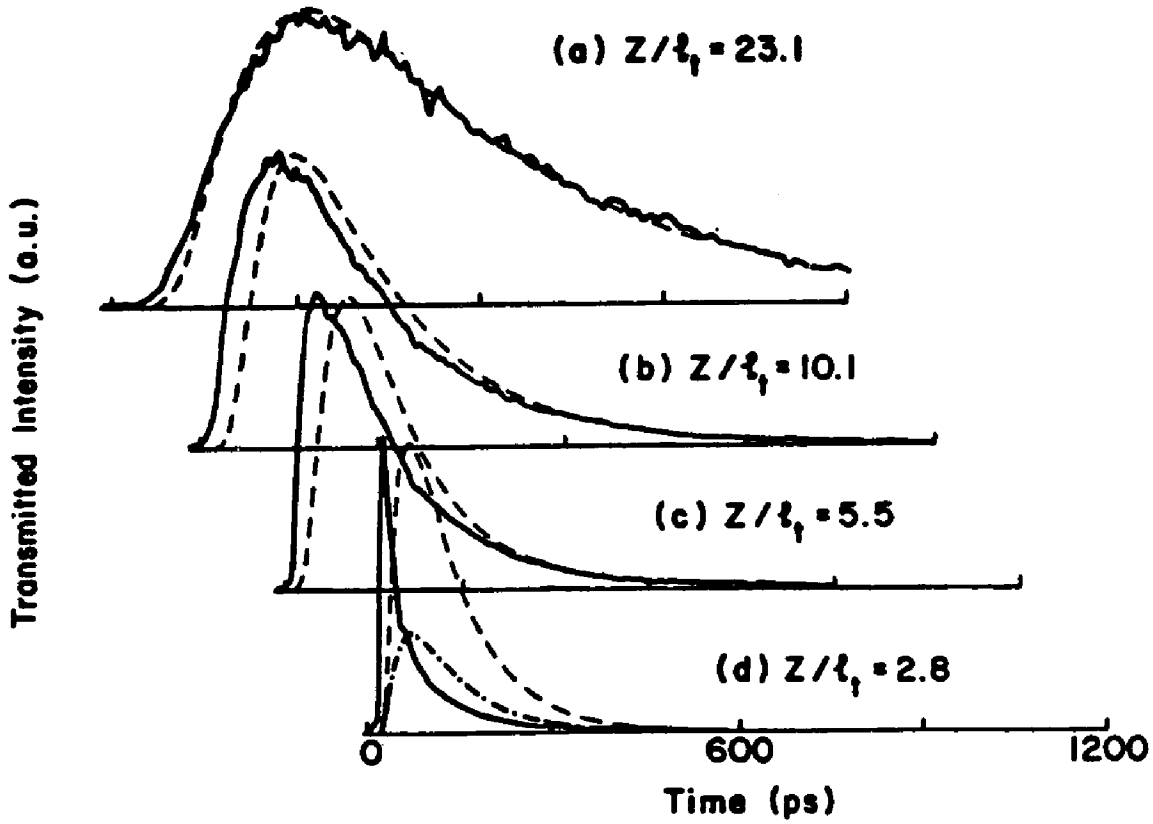

Fig.6.3 Transmitted pulse profiles of $10mm$ thick random media consisting latex beads of $3.134\mu m$ diameter. The bead concentrations n, l_t and z / l_t are: (a) $9.62\times10^5 mm^{-3}$, $0.433mm$ and 23.1; (b) $4.20\times10^5 mm^{-3}$, $0.989mm$ and 10.1; (c) $2.28\times10^5 mm^{-3}$, $1.823mm$ and 5.5; and (d) $1.16\times10^5 mm^{-3}$, $3.578mm$ and 2.8; respectively. Solid curves are the experimental results, broken and dash-dot curves are computed from the diffusion theory where the peak and total intensity are normalized, respectively.

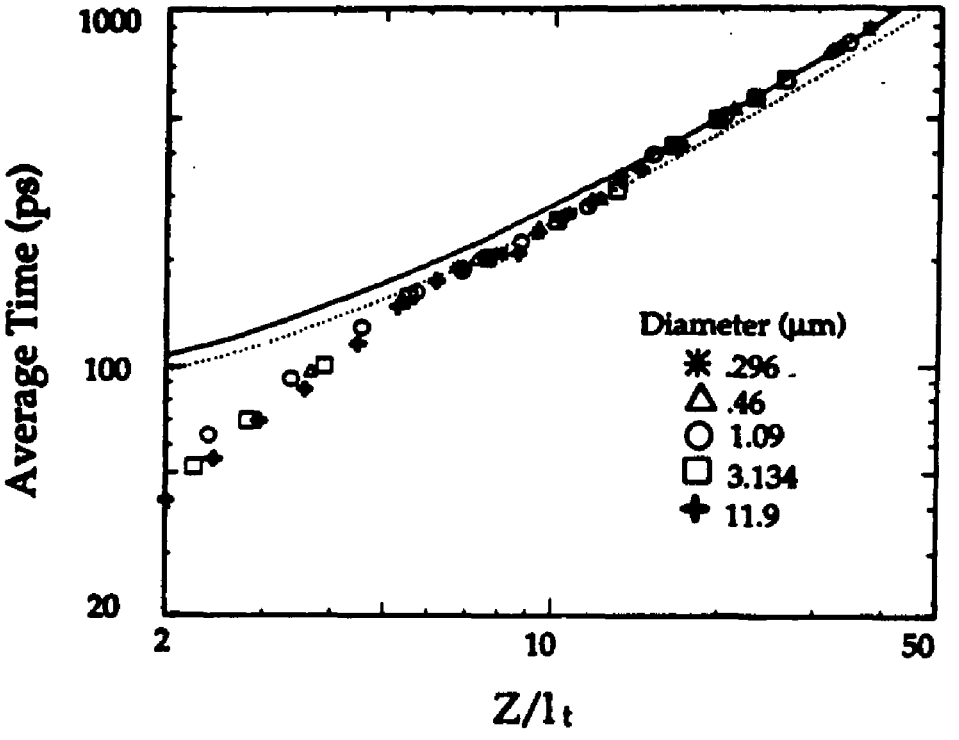

Fig.6.4 Plots of average time of arrival $\bar{t}$ versus z / l_t. Solid curve is the $\bar{t}$ predicted by diffusion theory, and the dotted curve is $0.9\bar{t}$. Experimental results (corresponding bead diameter) are plotted by star ($0.296\mu m$) triangle ($0.46\mu m$), octagon ($1.09\mu m$), square ($3.134\mu m$) and rose ($11.9\mu m$).

References

[1] Y. Kuga and A. Ishimaru, J. Opt. Soc. Am. A1, 831 (1984)

[2] M. P. Van Albada and Ad Lagendijk, Phys. Rev. Lett. 55, 2692 (1985)

[3] P.-E. Wolf and G. Maret, Phys. Rev. Lett. 55, 2696 (1985)

[4] A. A. Golubentev, Sov. Phys. JETP 59, 26 (1984)

[5] E. Akkermans, P. E. Wolf and Maynard, Phys. Rev. Lett. 56, 1471 (1986)

[6] L. Tsang and A, Ishimaru, J. Opt. Soc. Am. A 2, 1331 (1985)

[7] M. J. Stephen, Phys. Rev. Lett. 56, 1809 (1986)

[8] M. J. Stephen and G. Cwilich, Phys. Rev. B 34, 7564 (1986)

[9] D. Schmeltzer and M. Kaveh, Phys. Rev. B 36, 2251 (1988)

[10] E. Akkermans, P. E. Wolf, R. Maynard and G. Maret, J. Phys. France 49, 77 (1988)

[11] F. C. MacKintosh and S. John, Phys. Rev. B 37, 1884 (1988)

[12] M. B. van der Mark, M. P. van Albada, and Ad Lagendijk, Phys. Rev. B 37, 3575 (1988)

[13] S. Etemad, R. Thompson, and M. J. Andrejco, Phys. Rev. Lett. 57, 575 (1986)

[14] M. Kaveh, M. Rosenbluh, I. Edrei, and I. Freund, Phys. Rev. Lett. 57, 2049 (1986)

[15] M. P. van Albada, M. B. van der Mark, and Ad Lagendijk, Phys. Rev. Lett. 58, 361 (1987)

[16] A. Z. Genack, Phys. Rev. Lett. 58, 2043 (1987)

[17] S. Etemad, R. Thompson, M. J. Andrejco, Sajeev John and F. C. Mackintosh, Phys. Rev. Lett. 59, 1420 (1987)

[18] P. E. Wolf, G. Maret, E. Akkermans and R. Maynard, J. Phys. France 49, 63 (1988)

[19] R. Vreeker, M. P. van Albada, R. Sprik, and A. Lagendijk, Phys. Lett. A 132, 51 (1988)

[20] M. Rosenbluh, I. Edrei, M. Kaveh, and I. Freund, Phys. Rev. A 35, 4458 (1987)

[21] S. Etemad, Phys. Rev. B 37, 3652 (1988)

[22] Y. Kuga, L. Tsang and A. Ishimaru, J. Opt. Soc. Am. A 2, 616 (1985)

[23] M. Abramowitz and I. A. Stegun, Handbook of Mathematical Functions, Dover (1960), Pg. 686

[24] G. H. Watson, Jr., P. A. Fleury, and S. L. McCall, Phys. Rev. Lett. 58, 945 (1987)

[25] G. A. Navarro, and A. E. Profio, Med. Phys. 15, 181 (1988) Appl. Opt. 28, 2343 (1989)

[26] K. M. Yoo, K. Arya, G. C. Tang, J. L. Birman, and R. R. Alfano, Phys. Rev. A 39, 3728 (1989)

[27] K Shimizu, A. Ishimaru, L. Reynolds, and A. P. Bruckner, Appl. Opt. 18, 3484 (1979)

[28] K. M. Yoo, Y. Takiguchi, and R. R. Alfano, Appl Opt. 28, 2343 (1989)

[29] K. M. Yoo and R. R. Alfano, Opt. Lett. , March-1st-1990

[30] A. Ishimaru, and K. J. Painter, Radio Sci. 15, 87 (1980)

[31] R. Vreeker, M. P. van Albada, R. Sprik, and A. Lagendijk, Opt. Comm. 70, 365 (1989)

[32] R. L. Cheung, and A. Ishimaru, Appl. Opt. 21, 3792 (1982)

[33] J. M. Drake and A. Z. Genack, Phys. Rev. Lett. 63, 259 (1989)

[34] Y. Kuga, L. Tsang and A. Ishimaru, J. Opt. Soc. Am. A 2, 616 (1985)

[35] M. P. van de Albada, and Ad Lagendijk, Phys. Rev. B 36, 2353 (1987)

[36] S. Etemad, Phys. Rev. B 37, 3652 (1988)

[37] I. Freud, M. Kaveh, and M. Rosenbluh, Phys. Rev. Lett. 60, 1130 (1988)

[38] D. J. Pine, D. A. Weitz, P. M. Chaikin, and E. Herbolzheimer, Phys. Rev. Lett. 60, 1134 (1988)

[39] S. Feng, C. Kane, P. A. Lee, and A. D. Stone, Phys. Rev. Lett. 61, 834 (1988)

[40] I. Freud, M. Rosenbluh, and S. Feng, Phys. Rev. Lett. 61, 2328 (1988)

[41] K. M. Yoo, Y. Takiguchi, and R. R. Alfano, IEEE Photonic Tech. Lett. 1, 94 (1989)

[42] M. Lax, V. Nayaramamurti, and R. C. Fulton, Laser Optics of Condense Matters, Edited by J. L. Birman, H. Z. Cummins, A. A. Kaplyanskii, (Plenum, New York) 229 (1987) Leningrad (1987), published by Plenum, New York

[43] A. Ishimaru, and S. T. Hong, Radio Sci. 10, 637 (1975)

[44] A. Ishimaru, Wave Propagation and Scattering in Random Media, Vol. 2, Academic Press (1978), Pg.318-324.

[45] M. J. Stephen, Phys. Rev. B 37, 1 (1988)

[46] D. A. Weitz, D. J. Pine, P. N. Pusey, and R. J. A. Tough, Phys. Rev. Lett. 63, 1747 (1989)

[47] K. M. Yoo, and R. R. Alfano, Optics Letters (March 1990)